

Gamma radiation spectroscopy and the $^{12}\text{C}(\alpha,\gamma)^{16}\text{O}$ reaction with DRAGON

Cassi J. Galt ^a

^a TRIUMF, 4004 Wesbrook Mall, Vancouver, BC, Canada V6T 2A3

Abstract

The astrophysically important $^{12}\text{C}(\alpha,\gamma)^{16}\text{O}$ reaction was recently re-enacted at TRIUMF using DRAGON. In this reaction a ^{12}C nuclei fuses with an alpha particle to form ^{16}O . Gamma rays are produced during the ^{16}O decay, and these were detected by an array of 30 hexagonal BGO scintillation detectors. The purpose of this project was to devise a method of identifying and quantifying the discrete components of the gamma radiation using the resulting gamma spectra. The devised method involves identifying potential ^{16}O decay paths and the discrete set of gamma energies associated with these paths, generating detector response functions for gamma radiation of these energies, and fitting a linear combination of these response functions to the experimental spectra. The fit coefficients represent the relative strengths of the contributions of each discrete component to the total spectrum. The method was tested on data taken at the 10.356 MeV resonance, at which ^{16}O is known to decay solely through the 6.917 MeV state. Knowing this, two potential decay paths were assumed, these being cascade decay through the 6.917 MeV and 7.117 MeV states. The goal was to test the method at correctly identifying gammas produced in decays through closely spaced states. The test was not successful, and the conclusion is that the method is very sensitive to detector gains and, lacking more accurate information about these gains, the devised method cannot be used to distinguish between gammas so close in energy. The next step in this project must be an effort to better determine detector gains.

1. Introduction

The $^{12}\text{C}(\alpha,\gamma)^{16}\text{O}$ reaction

Figure 1 illustrates the astrophysically important $^{12}\text{C}(\alpha,\gamma)^{16}\text{O}$ reaction, in which a ^{12}C nucleus fuses with an alpha particle to produce ^{16}O and one or more gamma rays. This reaction is an *astrophysical* one because it occurs in stars; and it is an *important* one because it plays a critical role in stellar evolution and the nucleosynthesis of the elements.

To better understand this importance, see Figure 2, a simple representation of stellar evolution. Stars are born inside nebulae, vast clouds of mostly hydrogen gas, and the life of a star consists of a number of stages in which heavier and heavier elements are fused out of the original hydrogen.

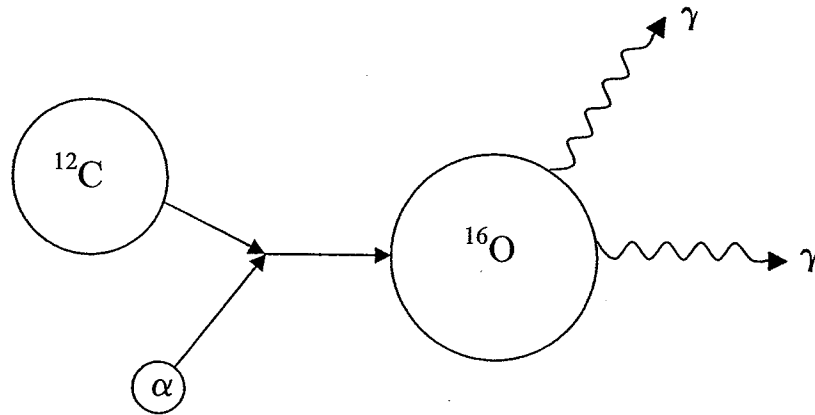


Figure 1: The astrophysically important $^{12}\text{C}(\alpha, \gamma)^{16}\text{O}$ reaction, in which a ^{12}C nucleus fuses with an alpha particle to produce ^{16}O and one or more gamma rays.

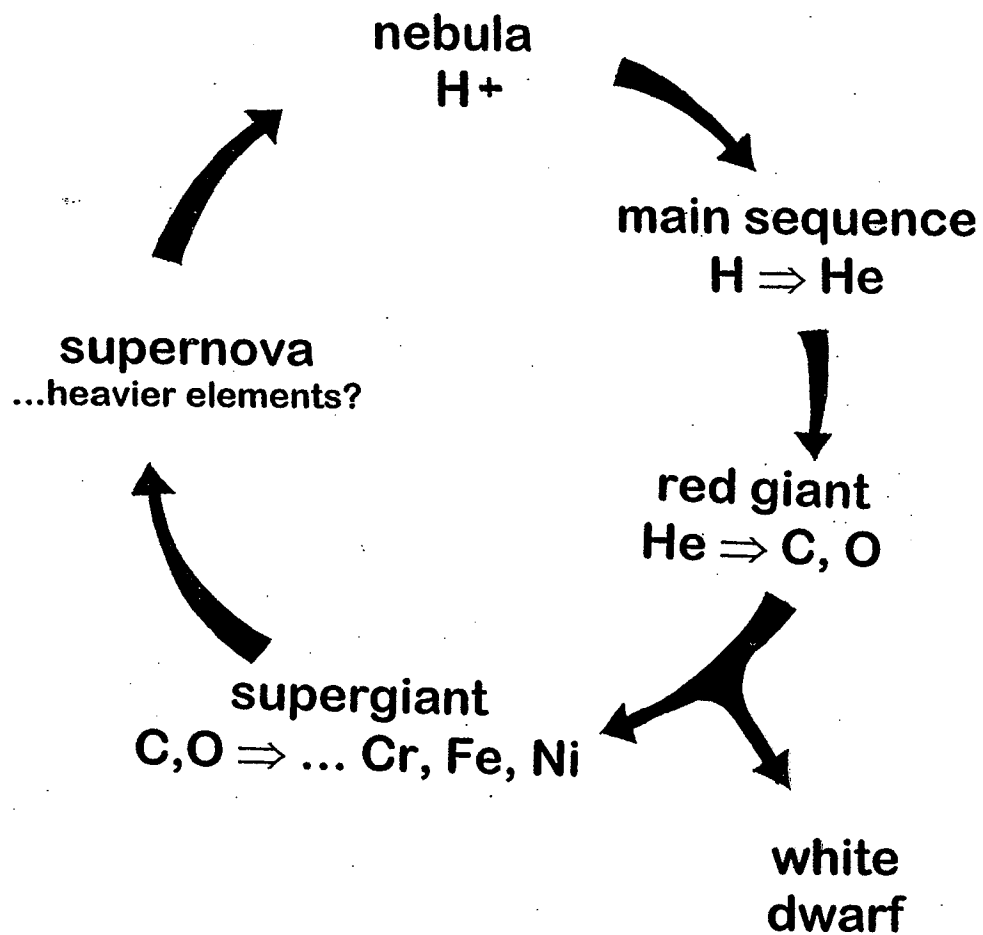


Figure 2: A simple representation of stellar evolution.

In the main sequence stage, hydrogen nuclei (protons) fuse to form helium nuclei; this is called hydrogen burning. In the red giant stage, helium nuclei fuse to form carbon and oxygen nuclei; this is called helium burning.

What happens next depends on the mass of the star. In very massive stars nucleosynthesis continues, with elements as heavy as those in the iron group being formed out of the carbon and oxygen ashes of helium burning. In less massive stars nucleosynthesis ceases with the formation of a white dwarf. The fate of very massive stars is generally a supernova event, a huge explosion in which all the elements formed inside the star are blown out into space. It is suspected that elements heavier than those in the iron group are formed during such explosions. The stellar matter rejoins the nebulae, ready to be formed into new stars and planets.

The $^{12}\text{C}(\alpha,\gamma)^{16}\text{O}$ reaction occurs during the helium burning stage. If one was to look inside the helium burning core of a star, one would see two reactions happening simultaneously: the triple- α reaction, by which carbon is formed via the fusion of three helium nuclei, and the $^{12}\text{C}(\alpha,\gamma)^{16}\text{O}$ reaction, by which carbon and helium fuse to form oxygen. These are illustrated in Figure 3.

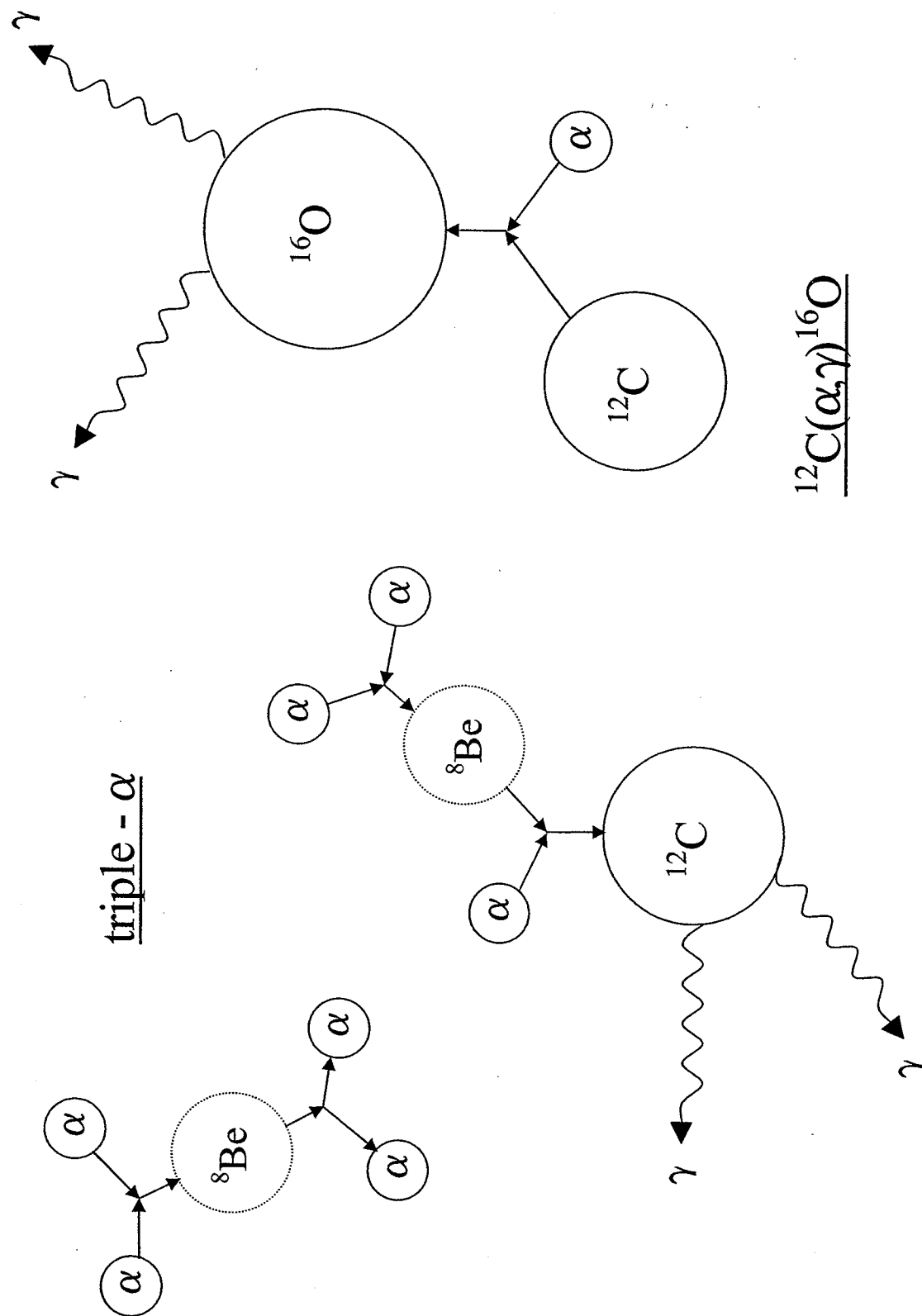
Given that this is where all of the carbon and all of the oxygen in the universe is synthesized, it is easy to see that there is an important relationship between the rates of these simultaneous reactions. If the $^{12}\text{C}(\alpha,\gamma)^{16}\text{O}$ reaction was to proceed much more slowly than the triple- α reaction, the universe would be very short on oxygen. And if it was to proceed much more quickly, the universe would be very short on carbon.

It is fortunate for all carbon-based, oxygen-breathing life forms (like humans) that both oxygen and carbon survive the helium burning phase in stars. It is also fortunate for the nucleosynthesis of all the heavier elements, for which the carbon and oxygen ashes of helium burning form the raw materials.

The triple- α process is well understood, but the $^{12}\text{C}(\alpha,\gamma)^{16}\text{O}$ reaction is not. In fact, the rate at which this reaction proceeds is currently one of the critical missing pieces in our understanding of stellar evolution and nucleosynthesis.

$^{12}\text{C}(\alpha,\gamma)^{16}\text{O}$ and DRAGON

Figure 3: The triple- α and $^{12}\text{C}(\alpha,\gamma)^{16}\text{O}$ reactions. These occur simultaneously during the helium burning stage of stellar evolution.



In order to better understand the $^{12}\text{C}(\alpha,\gamma)^{16}\text{O}$ reaction, physicists at TRIUMF recently re-enacted this stellar process using DRAGON (Detector of Recoils and Gammas of Nuclear Reactions).

Figure 4 is a schematic of the DRAGON experimental apparatus. A beam of ^{12}C nuclei is directed at a helium gas target, and these fuse with the helium nuclei to produce ^{16}O and one or two gamma rays. The DRAGON apparatus is, as its name suggests, able to detect both products of the reaction – the ^{16}O recoils and the gamma rays.

The gamma rays are detected by an array of 30 hexagonal bismuth germinate (BGO) scintillation detectors. These are packed around the helium target as shown in Figure 5.

Gamma radiation

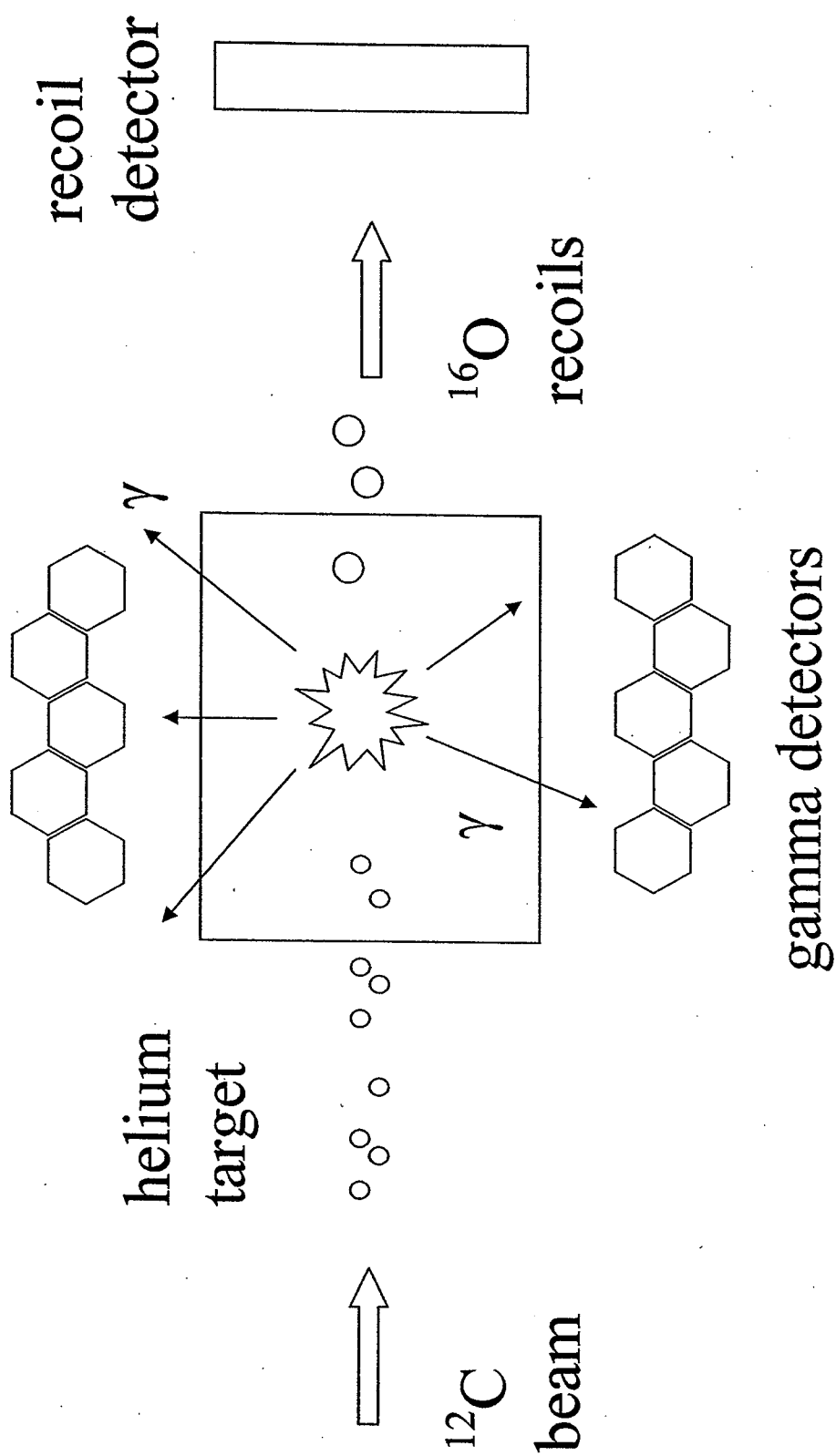
Where do these gamma rays come from? Immediately following the reaction the ^{16}O nucleus exists in an excited state, from which it soon decays to the stable ground state. Just like excited atoms emit photons of well defined energy upon de-excitation, excited ^{16}O nuclei emit gamma rays of well-defined energy upon decay.

The energy of the excited ^{16}O nucleus may be located on the ^{16}O energy level diagram in Figure 6. Some important features are labelled and discussed in Table 1.

a.	energy axis	The vertical axis is an energy axis. The bottom of the axis corresponds to zero energy, the ground state.
b.	resonant states	The $^{12}\text{C}(\alpha,\gamma)^{16}\text{O}$ resonant states are depicted by horizontal lines at the appropriate locations on the energy axis. Each resonant state has a certain angular momentum (J), parity (π), and energy (E_x). When the ^{16}O energy matches one of these resonant energies, the reaction yield reaches a peak.
c.	Q-value	The Q-value, 7.162 MeV, is the amount of energy released during the $^{12}\text{C} + \alpha$ fusion.

Table 1: Three important features in the ^{16}O energy level diagram.

Figure 4: A schematic of the DRAGON (Detector of Recoils and Gammas of Nuclear Reactions) experimental apparatus.



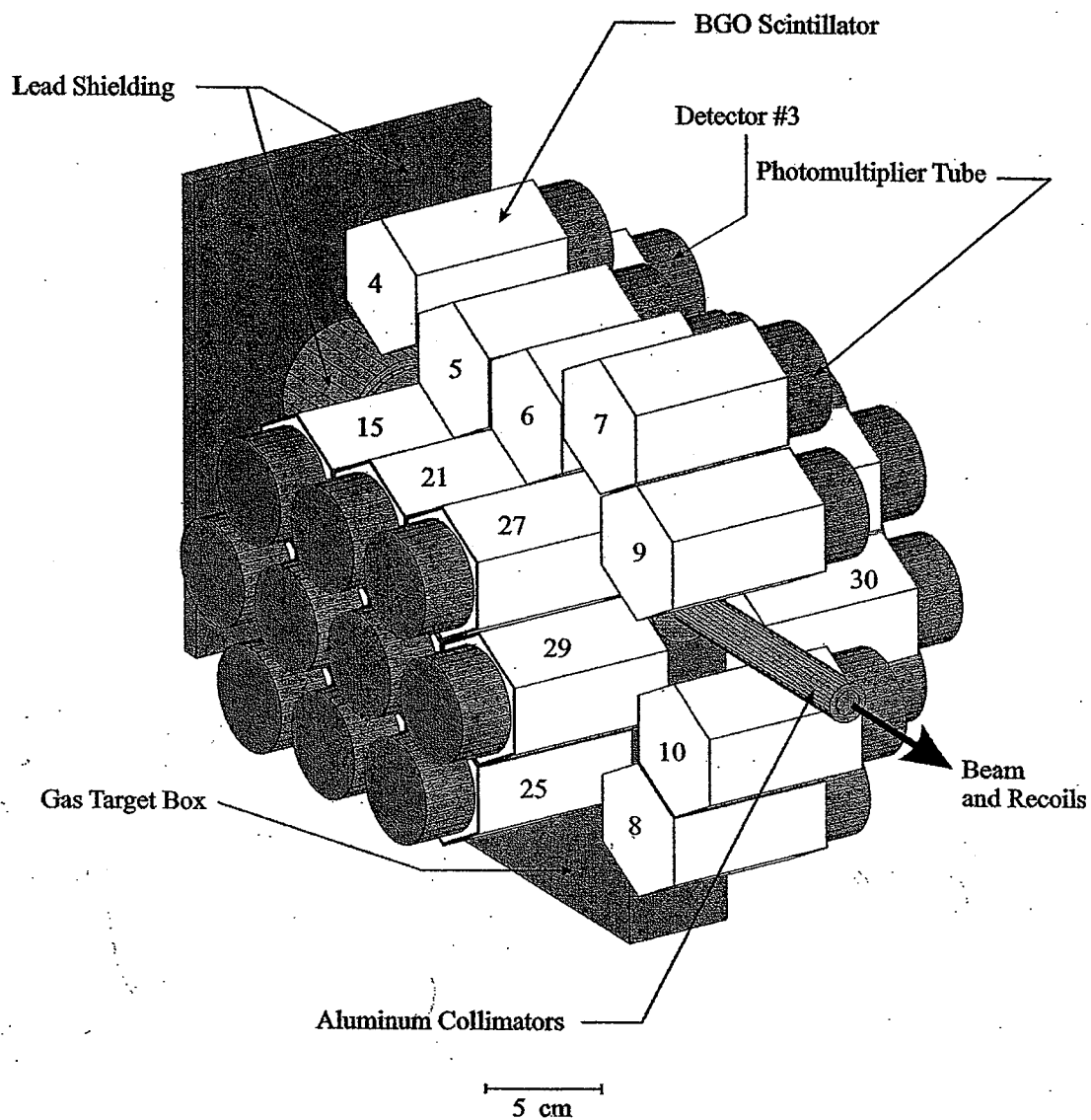


Figure 5: A schematic of the DRAGON gamma detector array. There are 30 hexagonal detectors made of bismuth germanate (BGO).

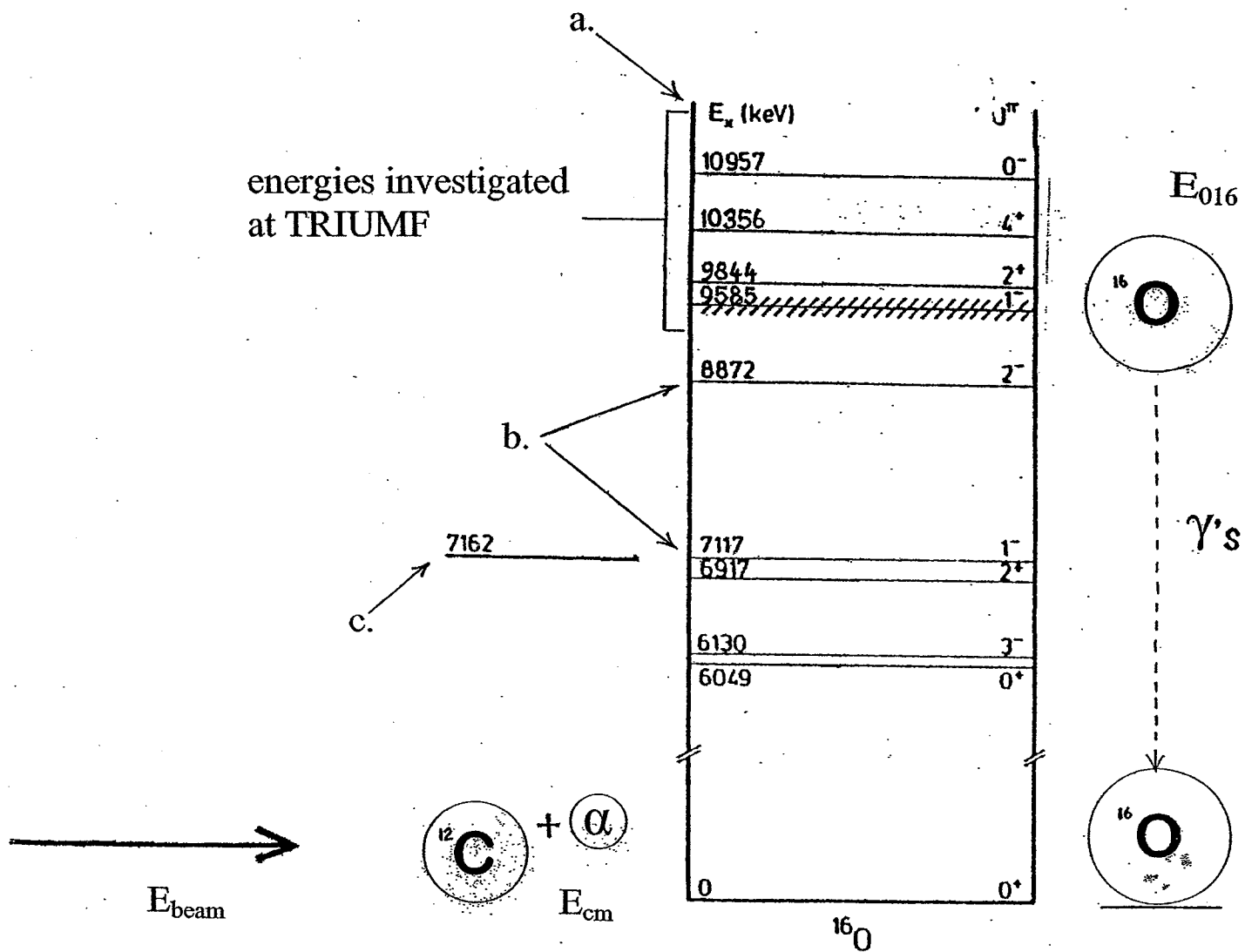


Figure 6: ^{16}O energy level diagram. The energy axis (a), $^{12}\text{C}(\alpha, \gamma)^{16}\text{O}$ resonant states (b), and reaction Q-value (c) are labelled. Also shown are the approximate range of energies investigated at TRIUMF and a sketch of the reaction nuclei. The energies E_{beam} , E_{cm} , and E_{016} are discussed in the text.

Figure 6 also includes a sketch of the reaction nuclei and their energies. Each ^{12}C beam particle has energy E_{beam} (often stated in units of MeV/u – to convert to MeV, just multiply by twelve). The energy of the $^{12}\text{C} + \alpha$ system in the center-of-mass frame, E_{cm} , is given by:

$$E_{\text{cm}} = E_{\text{beam}} \frac{A_{\alpha}}{A_{\alpha} + A_{^{12}\text{C}}} \quad (1)$$

Here, A is particle mass in amu. Finally, the energy of the product ^{16}O is given by the sum of the center-of-mass frame energy and the Q -value of the reaction:

$$E_{^{16}\text{O}} = E_{\text{cm}} + Q \quad (2)$$

It is important to realize that the ^{12}C nuclei lose energy as they travel through the helium target, and that the reaction may occur anywhere along the target length.

The approximate range of $E_{^{16}\text{O}}$ investigated at TRIUMF is indicated in Figure 6, extending from approximately 9.4 MeV to 11.7 MeV. Approximately 40 different energies were tested within this range, both on and in between the resonances, with gamma spectra collected at each.

The gamma spectra are simply histograms of detected gamma energy. Each gamma spectrum thus contains information about the energies and quantities of gammas produced during the ^{16}O decay. A sample spectrum, collected at the 10.356 MeV resonance, is shown in Figure 7.

Two major types of decay may be observed in any given gamma spectra: ground state and cascade. In a ground state decay, the ^{16}O nucleus decays directly to the stable ground state, emitting a single gamma ray of energy equal to the initial energy, $E_{^{16}\text{O}}$. In a cascade decay the ^{16}O nucleus decays first to one of the lower energy resonant states, and then to the ground state. Two gamma rays are emitted, their energies summing to the initial energy, $E_{^{16}\text{O}}$. Each gamma has energy equal to the difference between the initial and final state energies:

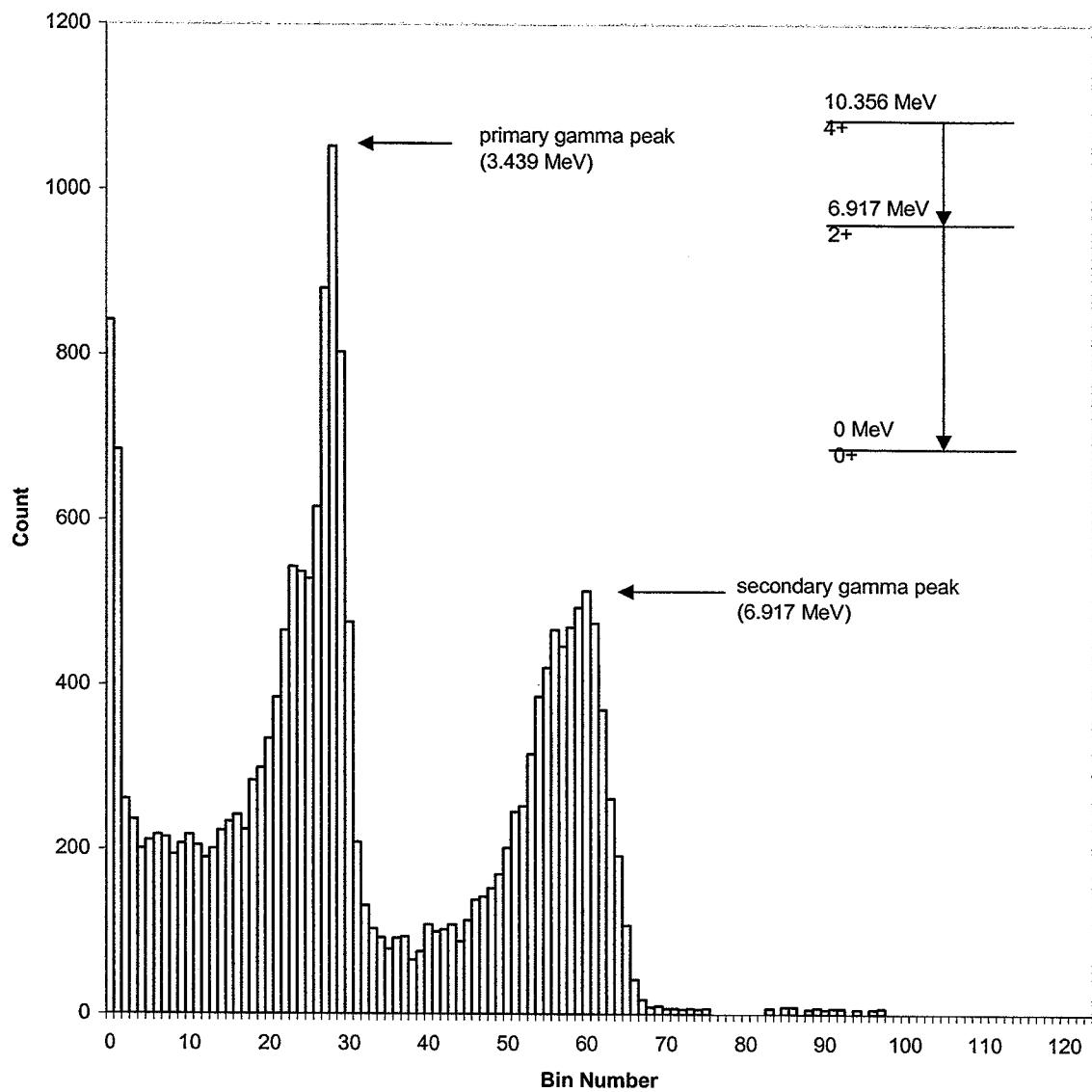


Figure 7: Gamma spectrum collected at the 10.356 MeV resonance (run # 8217, $E_{\text{beam}} = 1.067$ MeV/u). The primary and secondary gamma peaks are labelled.

$$E_{\gamma} = E_i - E_f \quad (3)$$

Depending on the energy E_{160} , more than one potential decay path may exist. These paths are not random, but must satisfy the energy, angular momentum, and parity conservation laws. It is impossible to know for certain which path a given ^{16}O nucleus will decay by, but it is possible to assign a probability to each decay path. Such a probability is called a branching ratio.

For E_{160} equal to one of the resonant state energies, the decay paths and probabilities are known, and are summarized in Table 2. For E_{160} falling in between the excited states, the decay paths and probabilities are not known.

The purpose of this project was to develop a method to extract these decay paths and probabilities from the gamma spectra. This is an application of *gamma radiation spectroscopy*, the study of the energy distribution of gamma rays. The resulting method, detailed below, was tested on the 10.356 MeV resonance spectrum of Figure 7.

2. Method

A three-step method was devised in answer to the question: how can the components of a gamma spectrum be identified and quantified? The first step is to identify potential decay paths and the set of discrete gamma energies associated with these paths. The second step is to generate a response function for each of these gamma energies. In this context a response function is simply a hypothetical gamma spectrum – the gamma spectrum that is expected to appear assuming monoenergetic gamma radiation. The third step is to fit the experimental spectrum with a linear combination of these response functions. The coefficients of such a fit may be interpreted as the relative strengths of the discrete components of the gamma spectrum.

These steps are discussed further below.

Identify potential decay paths

E_x (MeV ± keV)	Width Γ (keV)	Lifetime (s)	Cascade state (MeV)	Branching Ratio (%)
9.585 ± 11	420 ± 20	$(1.57 \pm 0.07) \times 10^{-21}$	0 6.917 7.117	63 ± 6 6 ± 6 31 ± 6
9.8445 ± 0.5	0.625 ± 0.100	$(1.0 \pm 0.2) \times 10^{-18}$	0 6.049 6.917	61 ± 4 18 ± 4 21 ± 4
10.356 ± 3	26 ± 3	$(2.5 \pm 0.3) \times 10^{-20}$	6.917	100
11.0967 ± 1.6	0.28 ± 0.05	$(2.4 \pm 4) \times 10^{-18}$	6.13 6.917	55 ± 23 45 ± 11
11.520 ± 4	71 ± 3	$(9.3 \pm 4) \times 10^{-21}$	0 6.049 6.917 7.117	91.7 4.2 ± 0.7 4.0 ± 1.0 < 0.8

Table 2: $^{12}\text{C}(\text{a,g})^{16}\text{O}$ resonant states, including state energies, state widths, lifetimes, decay paths, and branching ratios [1].

At the 10.356 MeV resonance, ^{16}O decay proceeds solely by cascade through the 6.917 MeV state (Table 2). Knowing this, two potential decay paths were assumed: cascade decay through the 6.917 MeV and 7.117 MeV states. The gamma energies associated with these decay paths are summarized in Table 3.

#	Decay type	Primary γ energy (MeV)	Secondary γ energy (MeV)
1	cascade	3.239	7.117
2	cascade	3.439	6.917

Table 3: Primary and secondary gamma energies for decays proceeding through the 6.917 MeV and 7.117 MeV states (10.356 MeV resonance)

The 6.917 MeV and 7.117 MeV states are separated by only 200 keV. This is a suitable test for the method, which must be able to distinguish between such closely spaced states if it is to be applied to gamma spectra of unknown composition.

Generate detector response functions

Next, response functions were generated for each of the gamma energies in Table 3. This was done on a detector by detector basis, knowing that each of the thirty BGO detectors has different gain and resolution properties. Three steps define the generation process:

i. GEANT simulation

A GEANT simulation of gamma detection within the BGO array was used to generate preliminary response functions at each of the important energies [2]. The simulation takes as input the number of gammas desired, the gamma ray energy, the location of the gamma source within the array, and the angular distribution of the gamma radiation. The simulation outputs, among other things, a histogram of the gamma energy detected within the BGO array – a gamma spectrum.

A note must be made about the strategy used to produce this spectrum. Within the simulation, any given gamma may deposit its energy in one or more of the thirty detectors. If energy is deposited in more than one detector, the simulation chooses the detector in which the most energy was deposited, and this energy *only* is included in the spectrum. Thus, the full gamma energy is not necessarily captured. This is called the *leading gamma method*¹.

The simulation was run for each of the important gamma energies. In each case, 100 000 events were simulated, and an isotropic angular distribution was assumed. The gamma source was located on a line extending the geometrical length of the target. This location was chosen after considering energy loss in the target and the width of the 10.356 MeV resonance; details are included in Appendix 1. Typical simulation output is shown in Figure 8 for gamma energy 6.917 MeV, detector 4.

The simulated spectrum does not represent the effects of detector gain and resolution. Thus, while such a spectrum is not a very good response function, it does provide a useful starting point.

ii. Detector resolution

It is undesirable but unavoidable that resolution varies from detector to detector. Upon commissioning, the best, worst, and average detector resolutions were found to be 6%, 7%, and 9% FWHM at 6.13 MeV [3].

For simplicity, the average resolution of 7% FWHM at 6.13 MeV was used for all detectors. Resolution is known to be energy dependent according to:

$$\text{FWHM} = k \sqrt{E} \quad (4)$$

¹ The leading gamma method must be used with care. When decay occurs via a cascade transition, two gamma rays are emitted almost simultaneously. If the leading gamma method is employed in such a case, the higher energy gamma ray will be represented preferentially in the gamma spectrum. This is not a problem in the simulations, which assume monoenergetic radiation, but can be a problem in the experimental data, which is also analyzed using the leading gamma method. To avoid this problem here, both the highest and the second highest energies detected among the thirty BGO detectors are included in the experimental gamma spectra. A consequence of this strategy is the presence of high counts in the lowest energy bins. Bins one through five were thus neglected throughout the analysis.

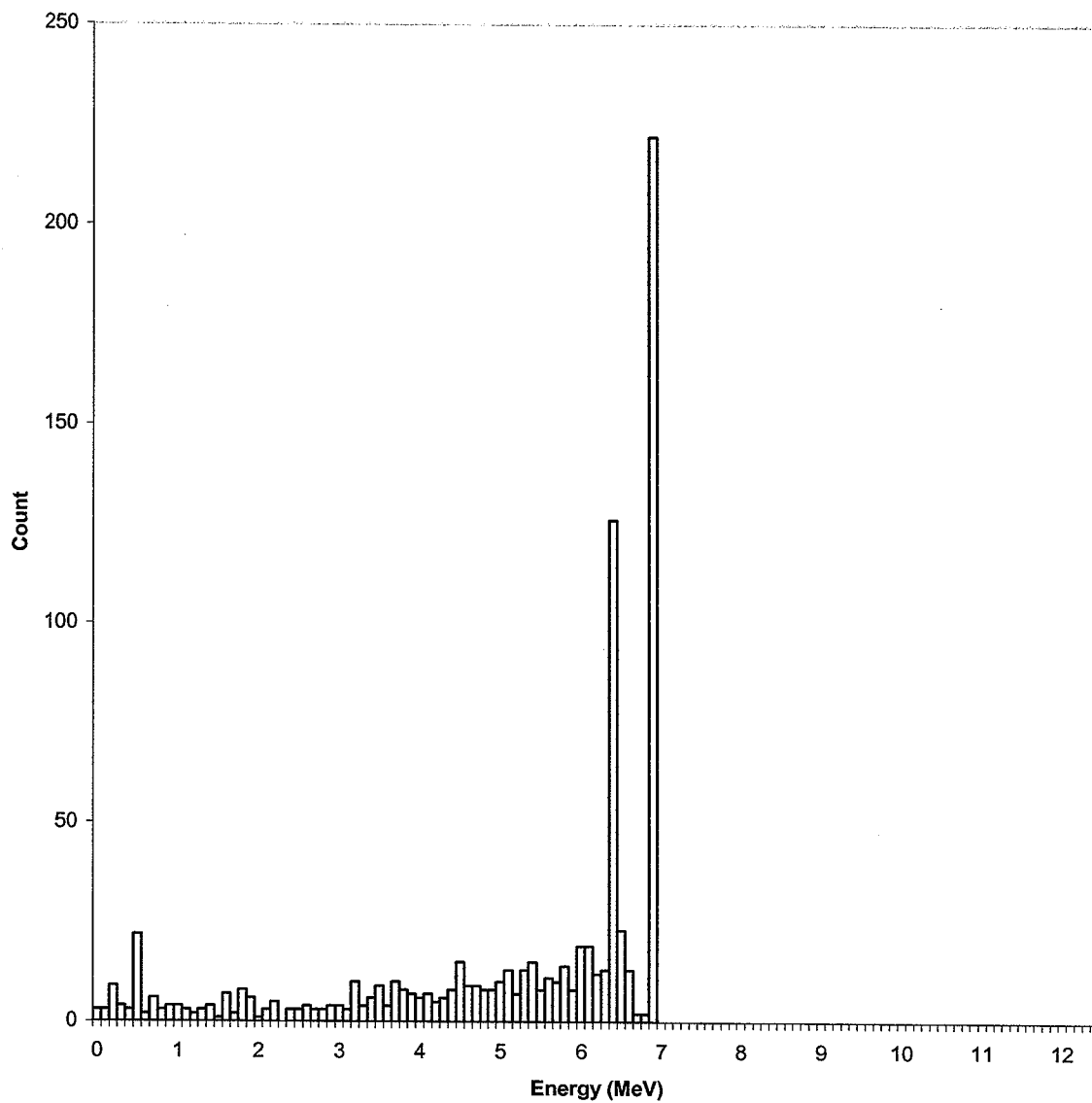


Figure 8: Typical gamma spectrum output by GEANT simulation. Shown is the spectrum observed at detector 4 for isotropic gamma radiation of energy 6.917 MeV.

For a 7% FWHM at 6.13 MeV, the constant k equals 0.173.

To incorporate detector resolution in the GEANT spectra, each preliminary response function was convolved with a Gaussian whose width varied with energy by the above formula. The code for this operation was written with Mathematica, and is included in Appendix 2.

Figure 9 shows the response function of Figure 8 as it appears after applying the Gaussian convolution.

iii. Detector gain

Like resolution, gain varies from detector to detector. The effect of detector gain is to map the gamma energy linearly to a histogram bin number:

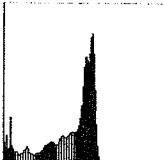
$$\text{Bin \#} = g E_{\gamma} + N \quad (5)$$

The 10.356 MeV resonance data has two distinct peaks at 3.439 MeV and 6.917 MeV. To determine g and N for each detector, the bin numbers of these peaks were identified by fitting Gaussians to the relevant portions of each detector's gamma spectrum. These fits are shown for detector 4 in Figure 10. The peak locations are plotted in Figure 11. A linear fit was performed using Minuit; the code and complete results are given in Appendix 3.

This mapping was then applied to each response function. Figure 12 shows the same response function for detector 4 after the mapping. Again, this operation was performed in Mathematica, and the code is given in Appendix 2.

iii. Fit response functions to experimental gamma spectrum

The final step is to fit the experimental gamma spectrum with a linear combination of the response functions. Symbolically:

$$\gamma \text{ spectrum} \leftrightarrow \sum c_i \text{  i$$

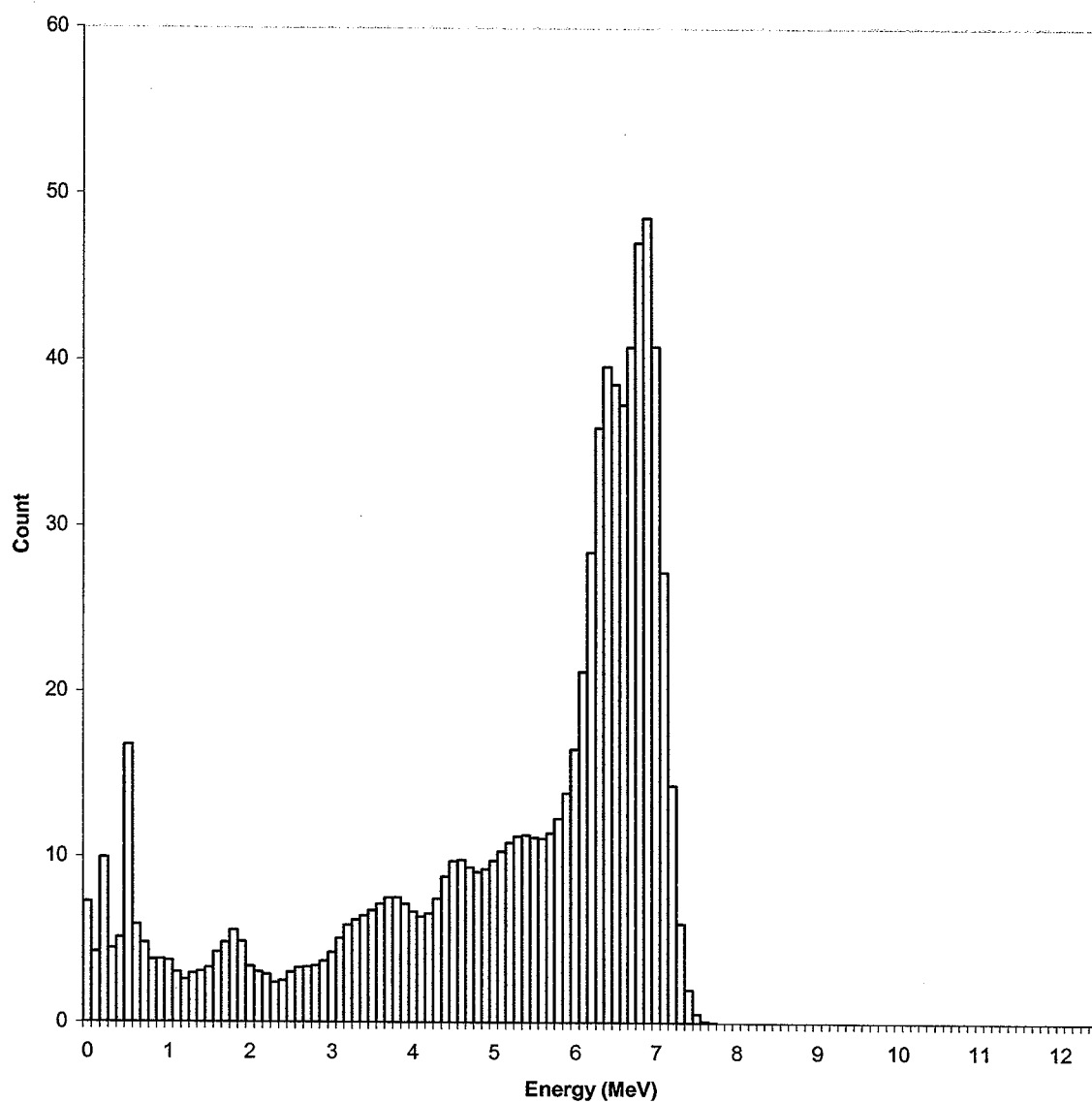


Figure 9: The same spectrum shown in Figure 8 (detector 4, 6.917 MeV gamma radiation) as it appears after applying the Gaussian convolution.

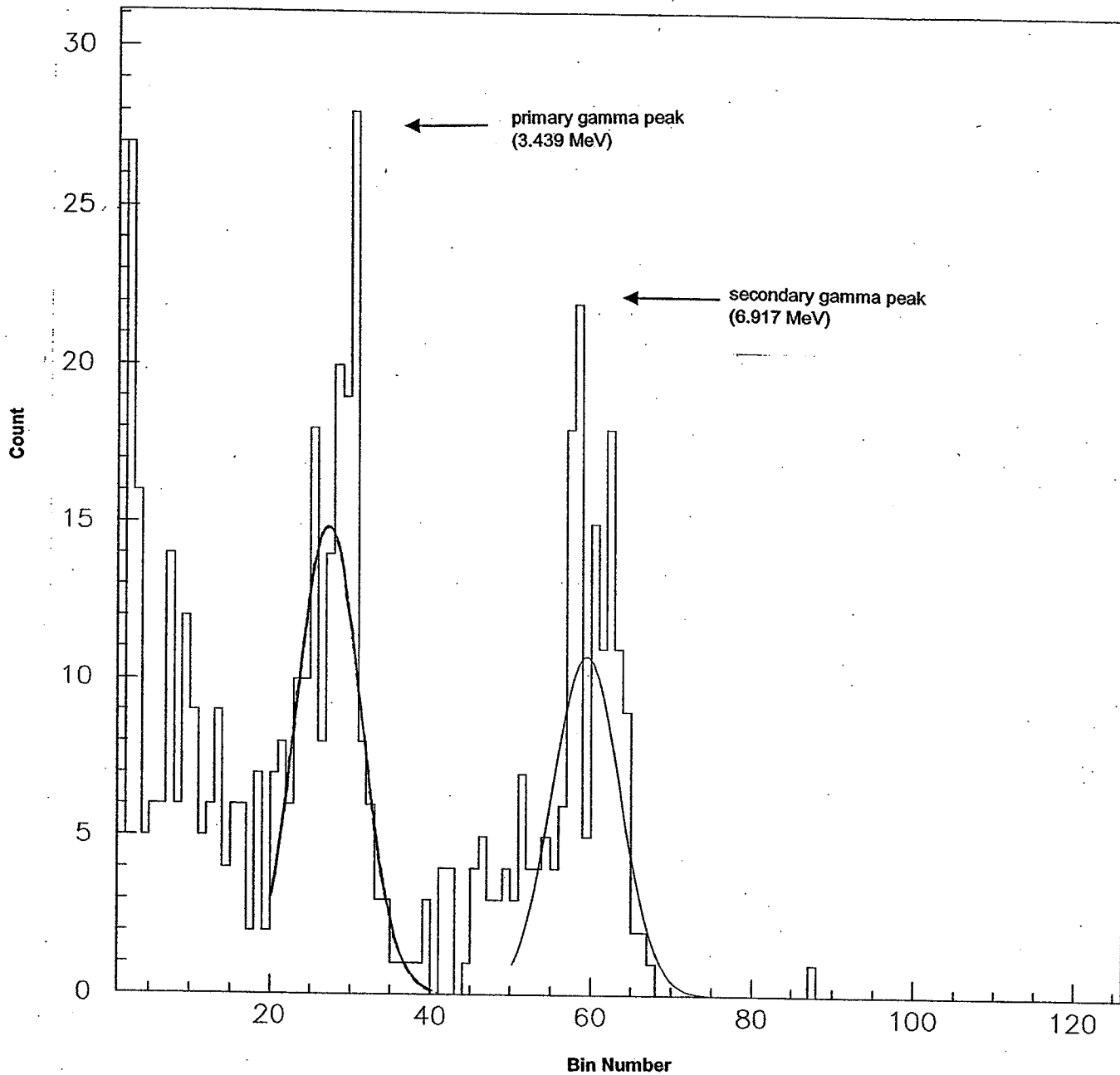


Figure 10: The experimental gamma spectrum observed at detector 4 and the Gaussian fits made to find the bin numbers of the primary and secondary gamma peaks. The Gaussian fits were made to bin numbers 20-40 and 50-80.

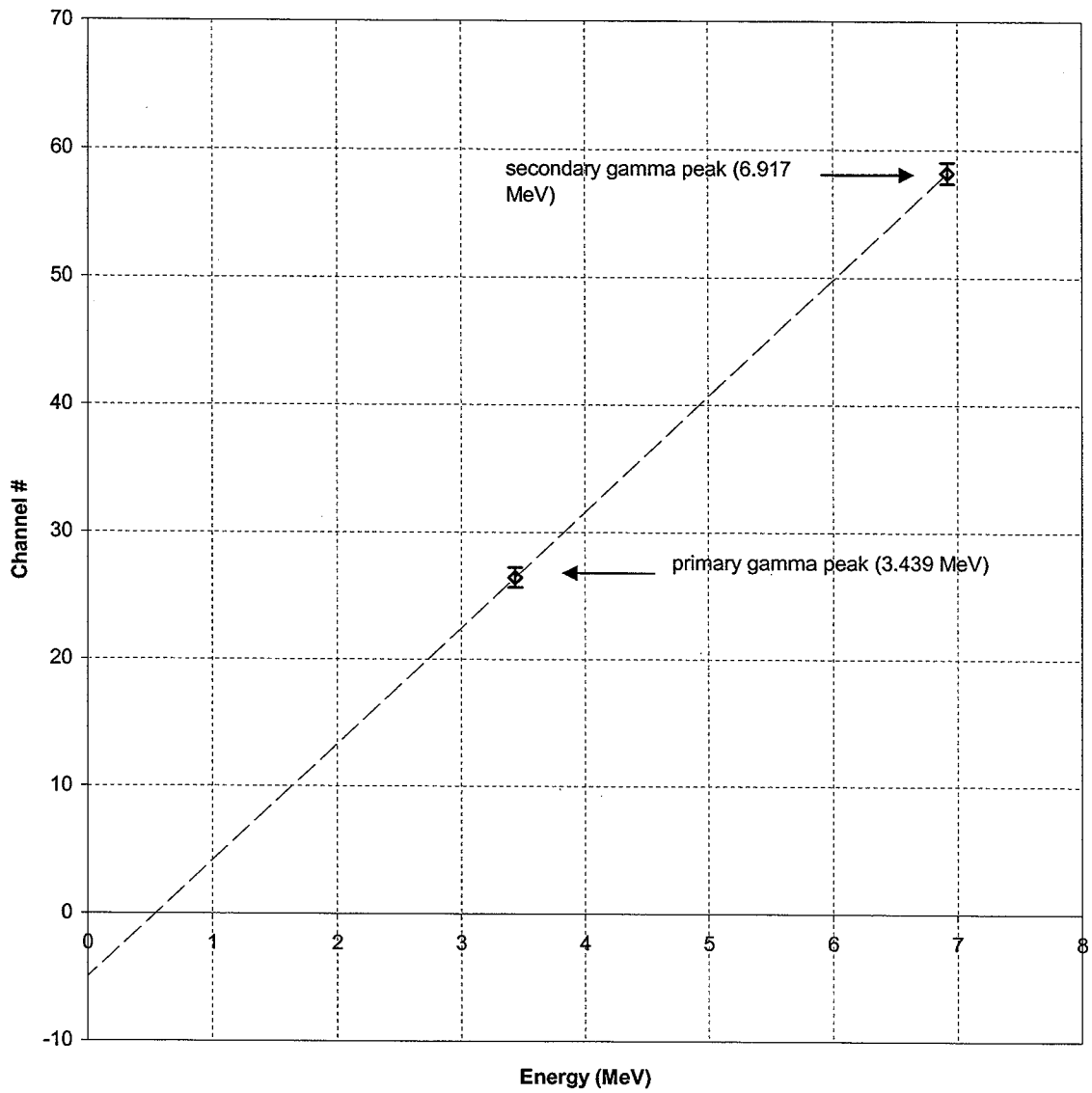


Figure 11: Plot of detector 4 primary and secondary gamma peak bin numbers. These were found using the Gaussian fits of Figure 10.

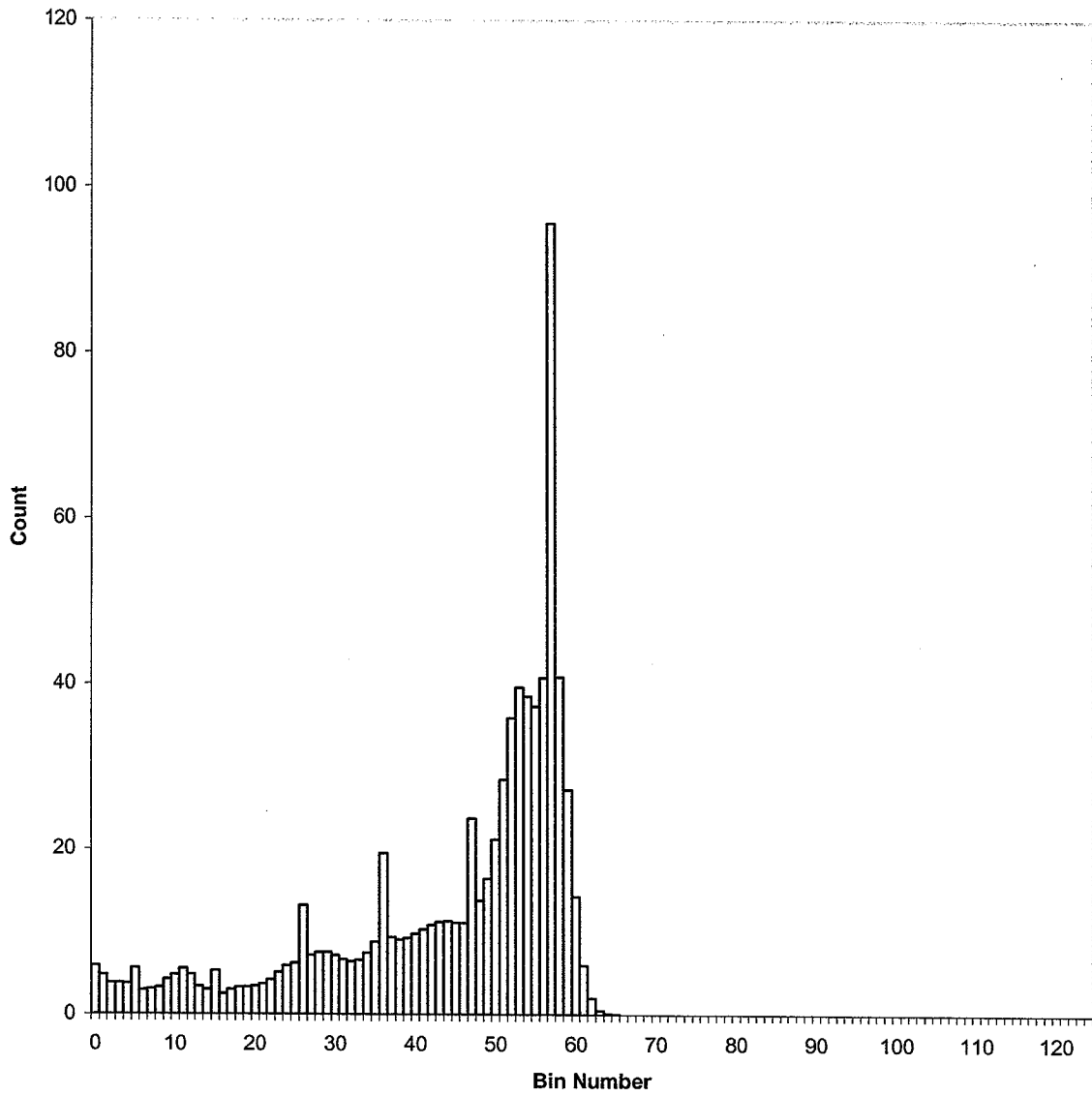


Figure 12: The same spectrum shown in Figure 8 (detector 4, 6.917 MeV gamma radiation) as it appears after applying the Gaussian convolution and the energy to bin number mapping.

Recall that the GEANT simulations assume isotropic gamma distribution. The real gamma radiation is not, in general, isotropic - the different energy gammas appear in different quantities in different regions of the BGO array.

One solution to this problem is to fit the gamma spectrum of each detector individually. This is not a good solution both because it is time consuming to perform thirty fits and because the number of counts recorded by single detectors is sometimes very small.

Instead, the thirty detectors were divided into five groups as shown in Figure 13. The experimental data and response functions were grouped accordingly. That is, if the response function for the j th detector and gamma energy E_γ is written r_{j, E_γ} , then the response function for the i th group and gamma energy E_γ is:

$$R_{i, E_\gamma} = N \sum r_{j, E_\gamma} \quad (6)$$

... where the sum is over the detectors in group i , and N is a normalization factor. Then the theoretical fit for the i th group to the experimental data, T_i , is written:

$$T_i = c_{i,1} R_{i,3.239} + c_{i,2} R_{i,7.117} + c_{i,3} R_{i,3.439} + c_{i,4} R_{i,6.917} \quad (7)$$

The total number of gammas of each energy that were simulated in GEANT, 100 000, was used as the normalization factor. This is not equal to the number of gammas detected by the simulation array, owing to the incomplete coverage of the gamma array and the efficiency of the BGO detectors.

A least squares fit was performed by minimizing the chi-square:

$$X^2 = \sum \frac{(E_k - T_k)^2}{\sigma_k^2} \quad (8)$$

Here, k represents bin number, and runs from one to 125. The one-standard-deviation error, σ_k , was simply taken to be the square root of the corresponding experimental data point, E_k . This minimization was performed with Minuit, and details are given in Appendix 4.

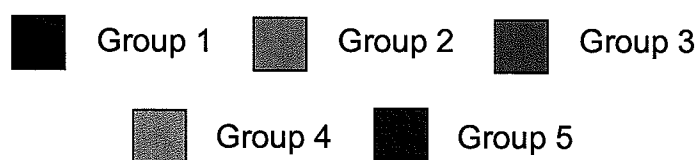
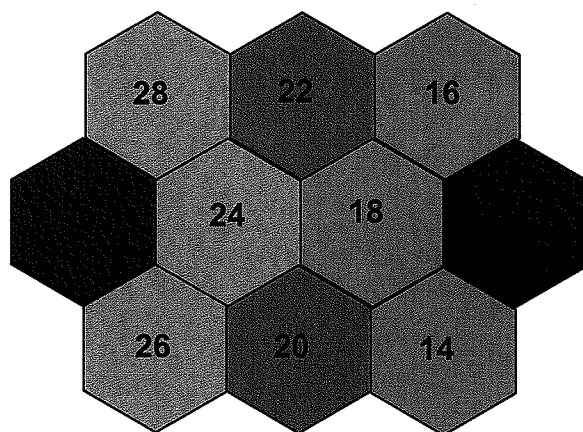
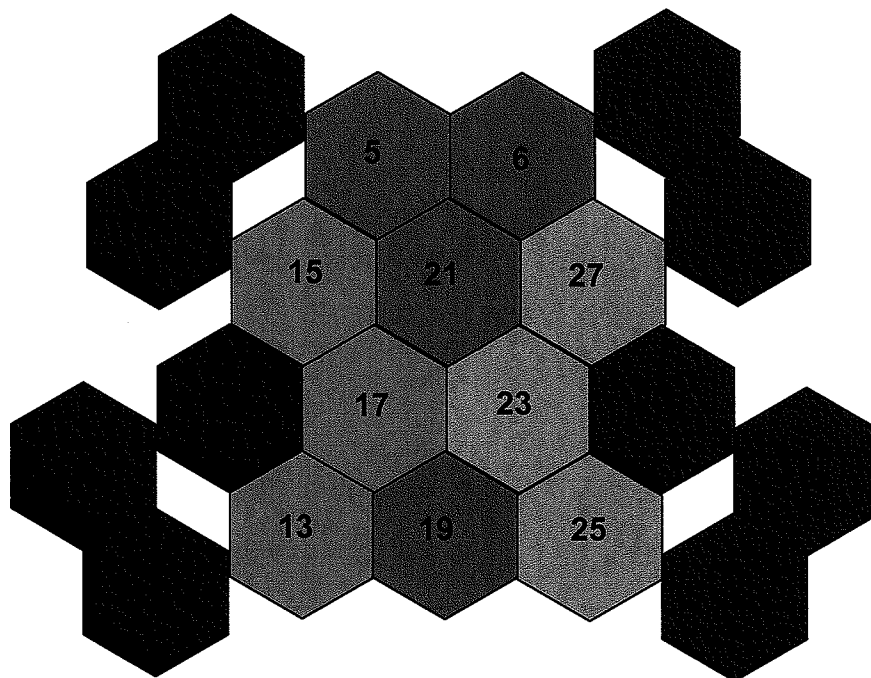


Figure 13: Detector groupings.

3. Results and Discussion

The fit coefficients and errors are given in Table 4, and the fits themselves are plotted against the experimental data in Figure 14.

Because of the way the response functions were normalized, the fit coefficients represent the number of gammas of each of the important energies that would actually have been generated in the reaction, had the reaction been isotropic. The sum of the coefficients obtained for a given group thus represents the total number of gammas generated in the reaction. Table 5 contains the percentage of this total attributable to each of the four important energy gammas. Figure 15 presents this information in pie charts.

It is known that decay from the 10.356 MeV resonance proceeds solely through the 6.917 MeV state. Thus, the coefficients for the 7.117 and 3.239 MeV gammas should be zero for all groups – that is, the pie charts should include no pink or red sections.

Clearly, the results do not satisfy this requirement. Although the fit correctly chooses the 3.439 MeV gammas over 3.249 MeV gammas, it incorrectly prefers the 7.117 MeV gammas to 6.917 MeV gammas.

Considering the plots of the fits in Figure 14, it appears that the detector gains are at fault here, being slightly too low in general. Possible reasons for this can be observed in the Gaussian fits of Figure 10. The two peaks are not true Gaussians, but have low energy tails that pull the fit down to lower bin numbers. This problem is exaggerated by the low counts existing in the tail bins, which, when the standard square-root-of-the-count standard deviation is used, give these points particularly high weight in the chi-square minimization.

To test this hypothesis, the fits were redone using the maximum g and N allowed within errors. The results are presented, as before, in Tables 6 and 7, and Figures 16, 17, and 18. Given these higher gains, the results are much closer to those expected, with the fitting procedure preferring the 3.439 MeV and 6.917 MeV gammas, as required.

Group #	3.239 MeV			7.117 MeV			3.439 MeV			6.917 MeV		
	Fit	-	+	Fit	-	+	Fit	-	+	Fit	-	+
1	0	at limit	1953	20283	-4804	4414	14242	-2162	1129	3692	at limit	4848
2	0	at limit	499	15179	-821	788	13178	-795	794	0	at limit	505
3	0	at limit	379	10550	-560	536	11479	-667	651	0	at limit	344
4	3405	-1081	1081	12337	-737	705	6004	-1125	1125	0	at limit	441
5	37	at limit	2551	26143	-1914	1723	15868	-2798	1359	0	at limit	1299

Table 4: Minuit fit coefficients and errors.

Group #	3.239 MeV	7.117 MeV	3.439 MeV	6.917 MeV
1	0	53 ± 16	37 ± 9	10 ± 13
2	0	54 ± 4	46 ± 4	0
3	0	48 ± 3	52 ± 4	0
4	16 ± 1	57 ± 6	28 ± 6	0
5	0	62 ± 8	38 ± 8	0

Table 5: Percentage of each of the four gamma energies present in the Minuit fits.

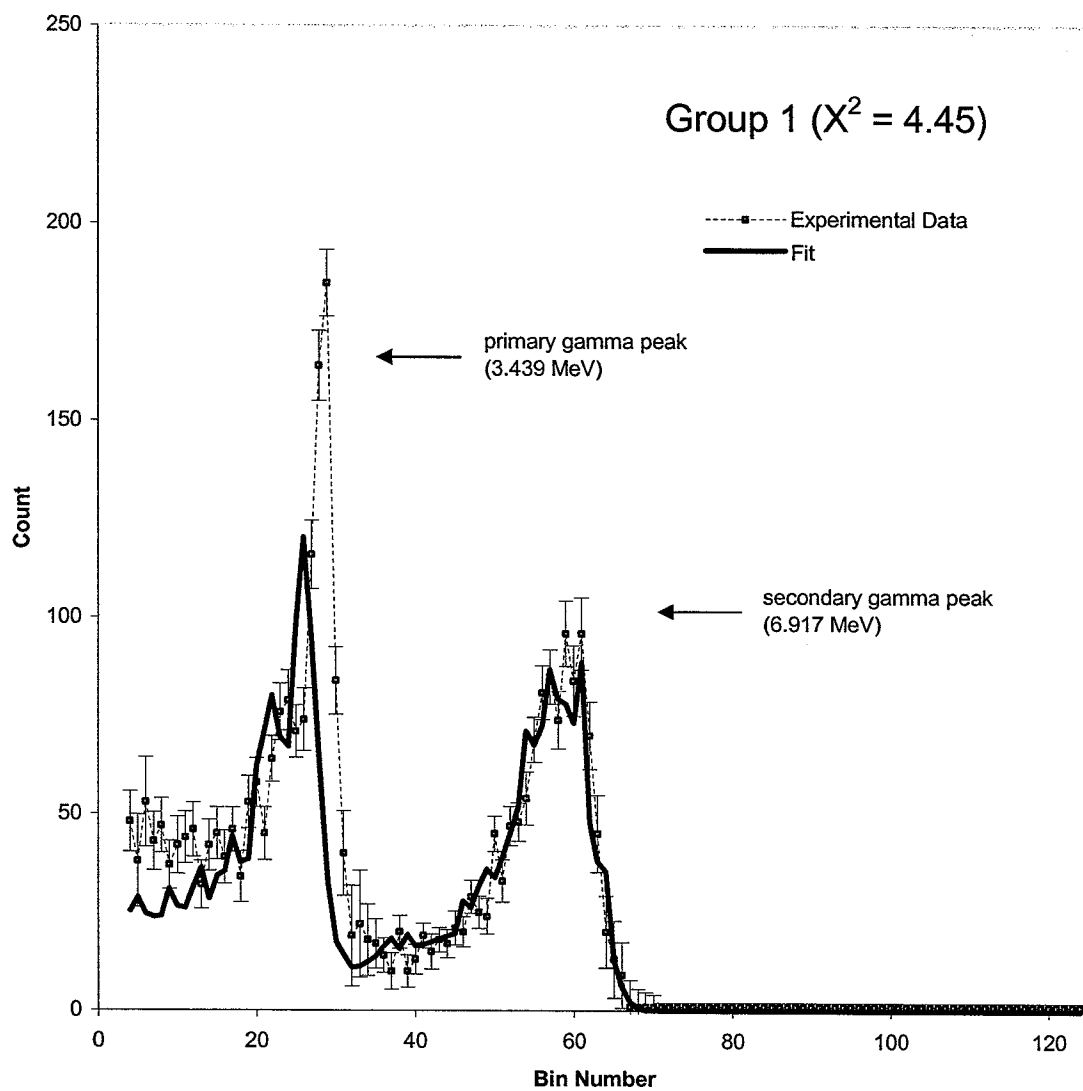


Figure 14a: Group 1 experimental spectrum and Minuit fit. Group 1 consists of detectors 1, 2, 3, 4, 11, and 12.

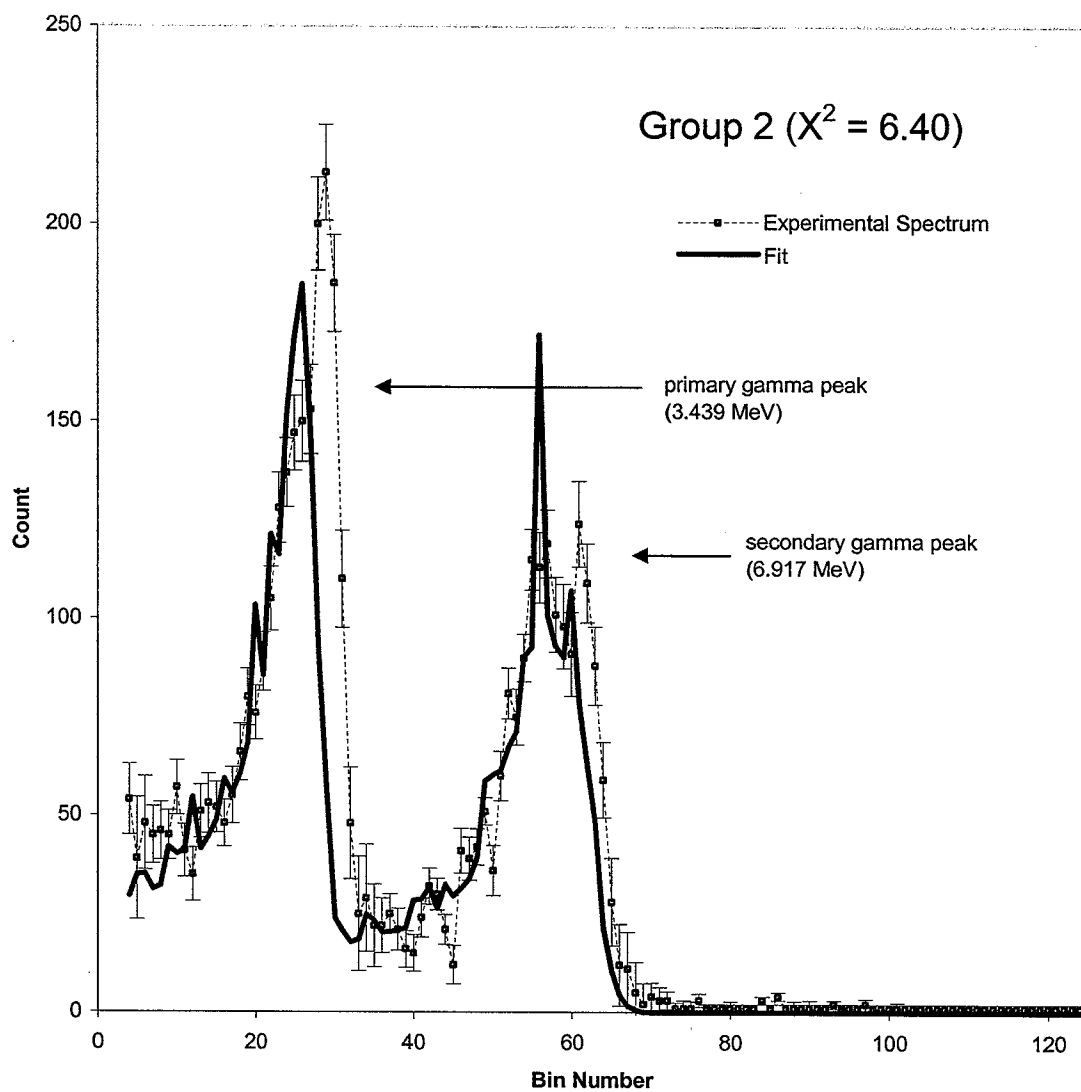


Figure 14b: Group 2 experimental spectrum and Minuit fit. Group 2 consists of detectors 13, 14, 15, 16, 17, and 18.

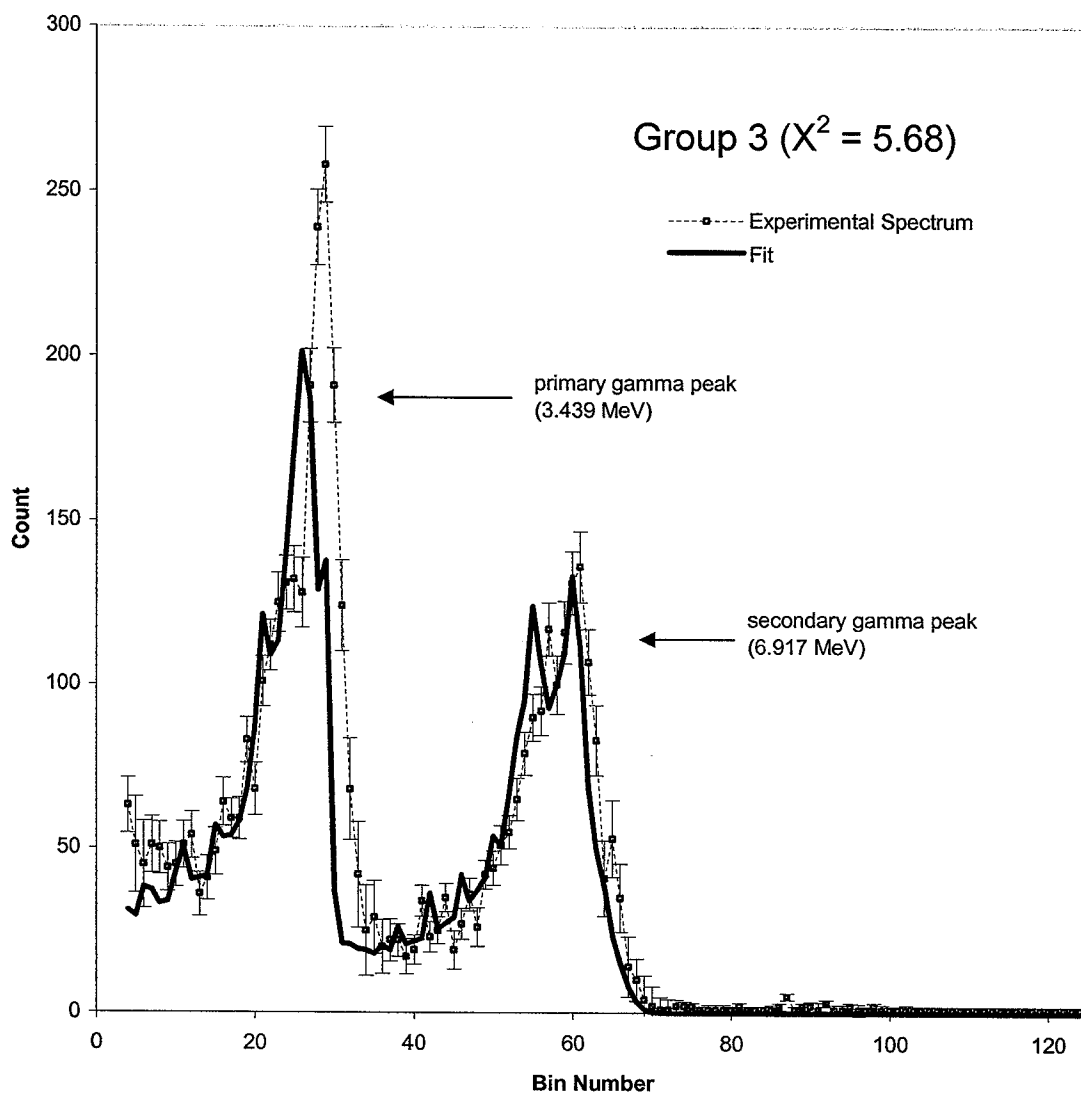


Figure 14c: Group 3 experimental spectrum and Minuit fit. Group 3 consists of detectors 5, 6, 19, 20, 21, and 22.

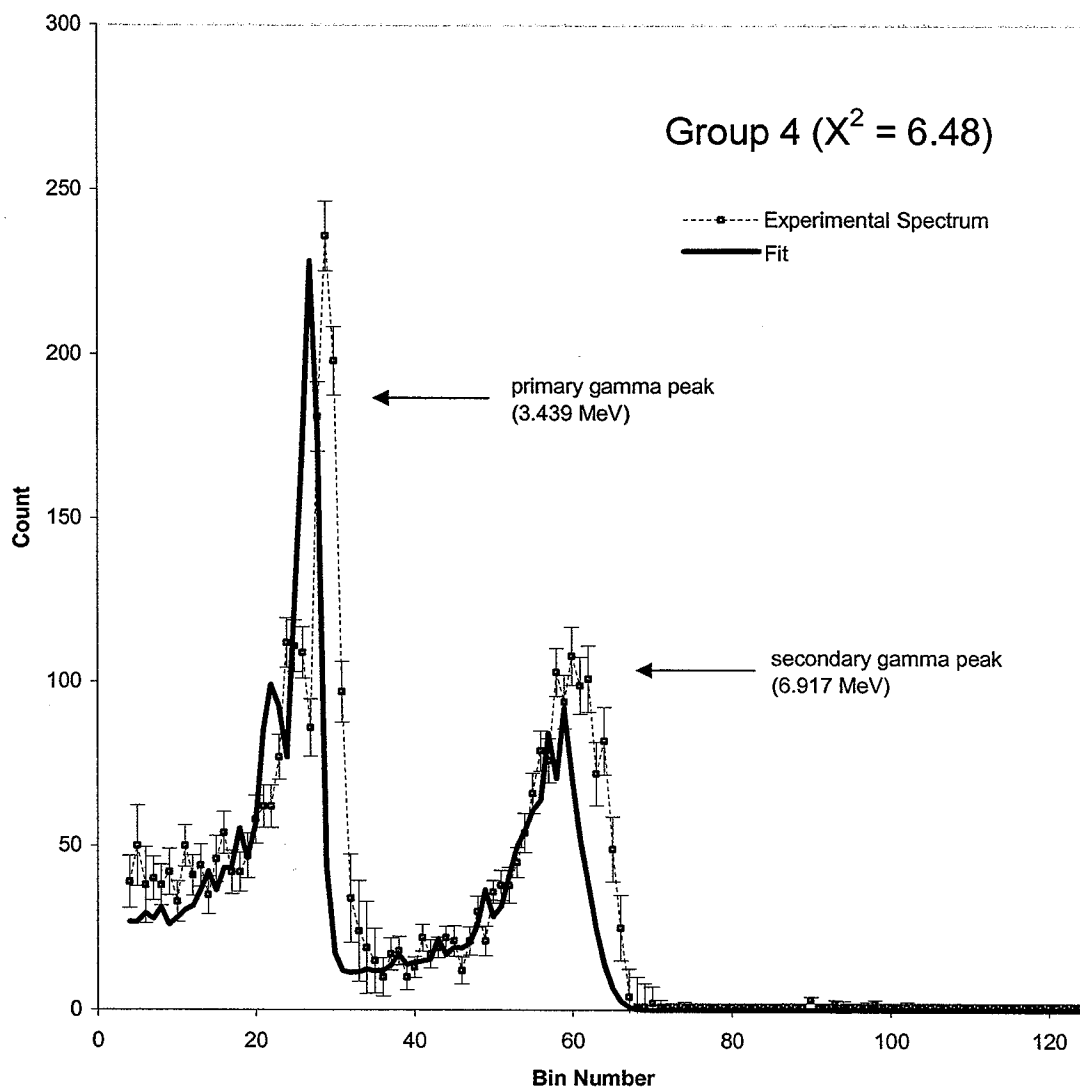


Figure 14d: Group 4 experimental spectrum and Minuit fit. Group 4 consists of detectors 23, 24, 25, 26, 27, and 28.

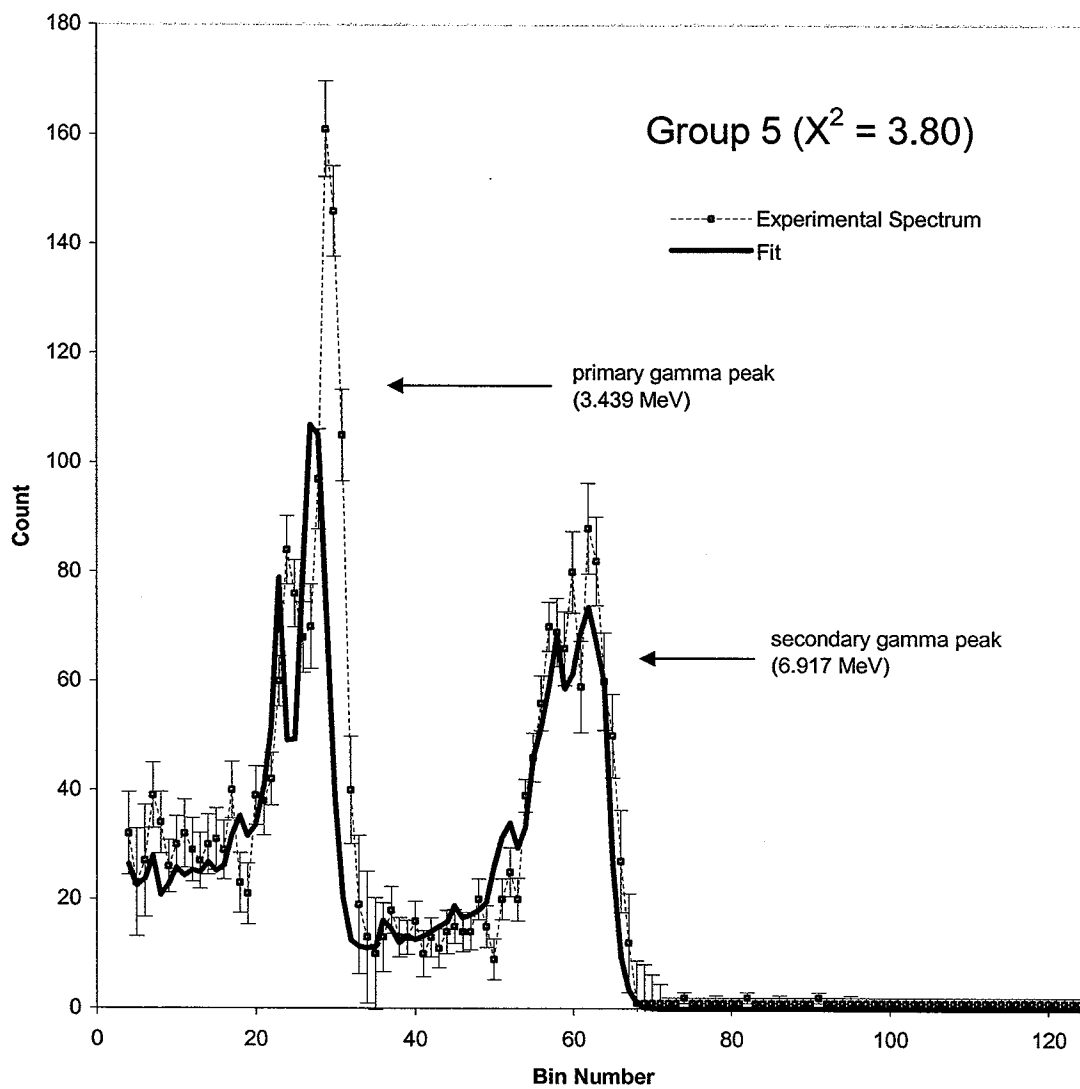


Figure 14e: Group 5 experimental spectrum and Minuit fit. Group 5 consists of detectors 7, 8, 9, 10, 29, and 30.

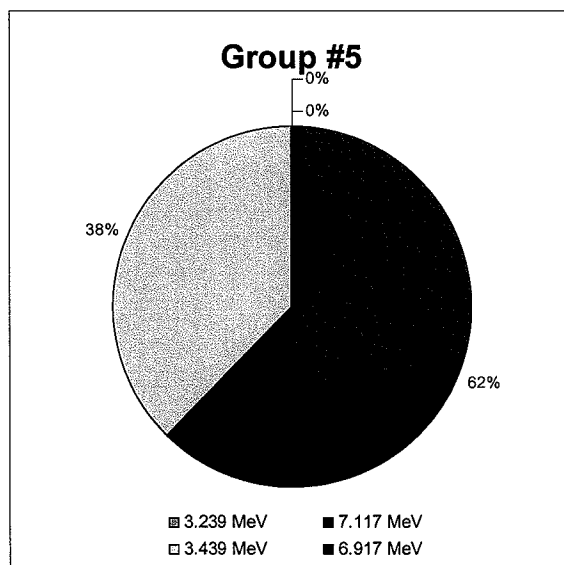
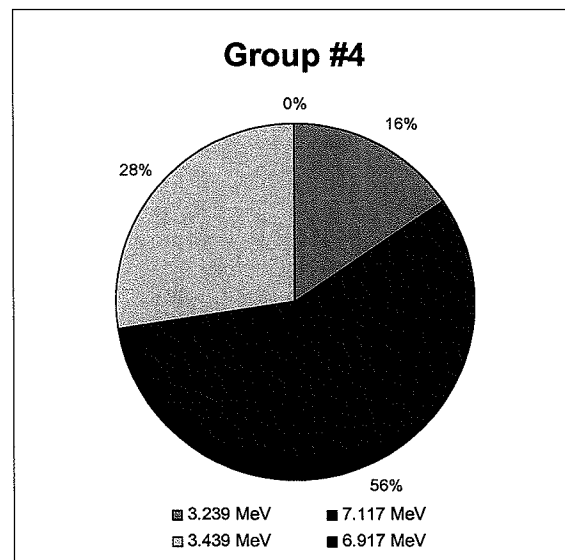
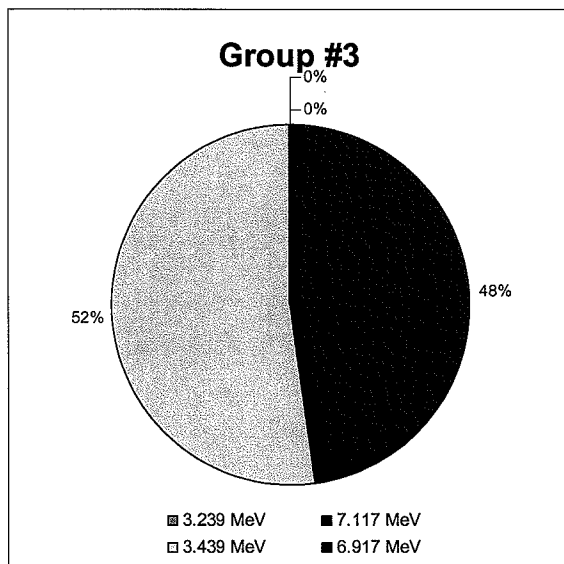
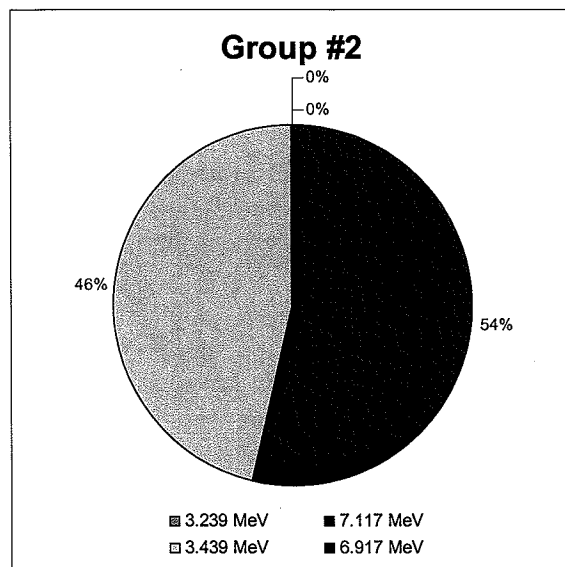
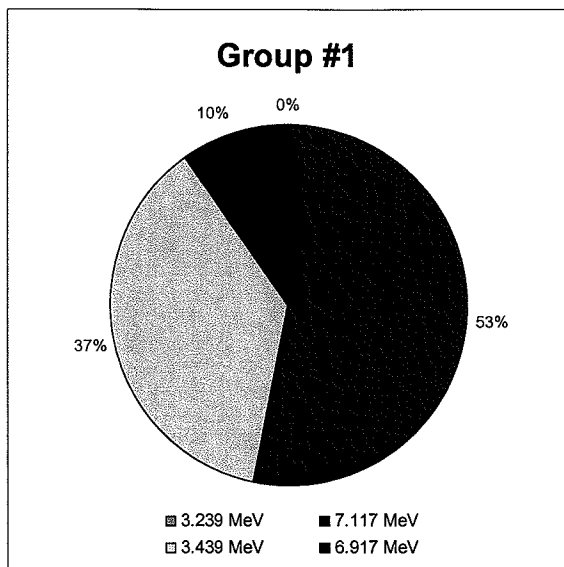


Figure 15: Pie charts showing percentage of each of the four gamma energies present in the fits to the five groups. At the 10.356 MeV resonance, ^{16}O decay is known to proceed solely through the 6.917 MeV state; thus only 3.439 MeV (light blue) and 6.917 MeV (dark blue) gammas should appear.

Group #	3.239 MeV			7.117 MeV			3.439 MeV			6.917 MeV		
	Fit	-	+	Fit	-	+	Fit	-	+	Fit	-	+
1	9246	-2484	2482	0	at limit	90	11557	-2513	2515	11880	-1043	1044
2	0	at limit	709	0	at limit	1366	16384	-1077	877	15159	-1542	797
3	1493	at limit	1736	0	at limit	337	12465	-1884	1867	10266	-571	543
4	0	at limit	759	0	at limit	422	14082	-1028	800	11692	-724	689
5	7869	-3084	3089	0	at limit	184	13512	-3219	3214	22250	-1632	1633

Table 6: Minuit fit coefficients and errors for fits done with maximum gains allowed within errors.

Group #	3.239 MeV	7.117 MeV	3.439 MeV	6.917 MeV
1	28 ± 8	0	35 ± 9	36 ± 5
2	0	0	52 ± 4	48 ± 5
3	6 ± 7	0	52 ± 10	42 ± 5
4	0	0	55 ± 5	45 ± 4
5	18 ± 7	0	31 ± 8	51 ± 7

Table 7: Percentage of each of the four gamma energies present in the Minuit fits for fits done with maximum gains allowed within errors.

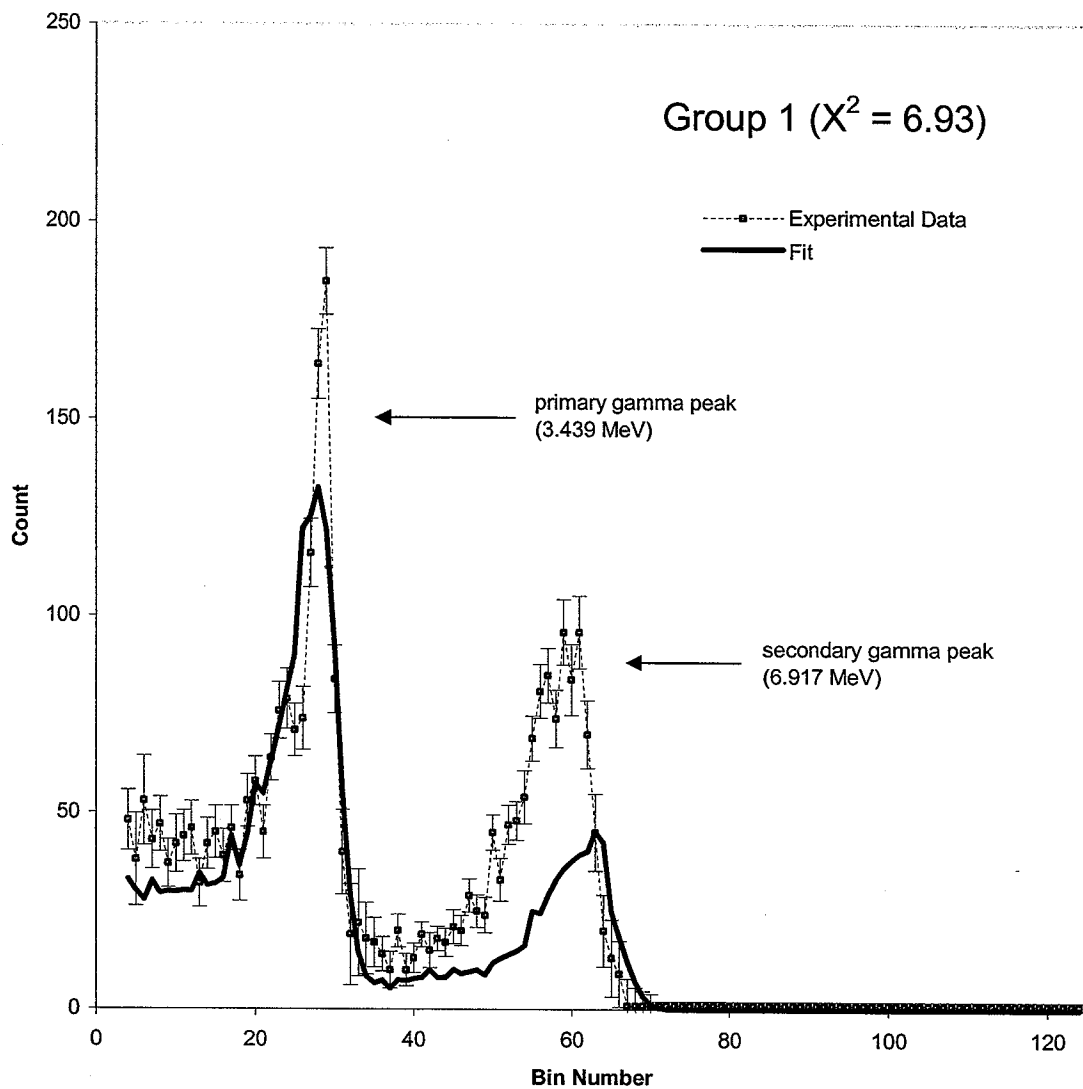


Figure 16a: Group 1 experimental spectrum and Minuit fit performed using maximum gains within allowed errors. Group 1 consists of detectors 1, 2, 3, 4, 11, and 12.

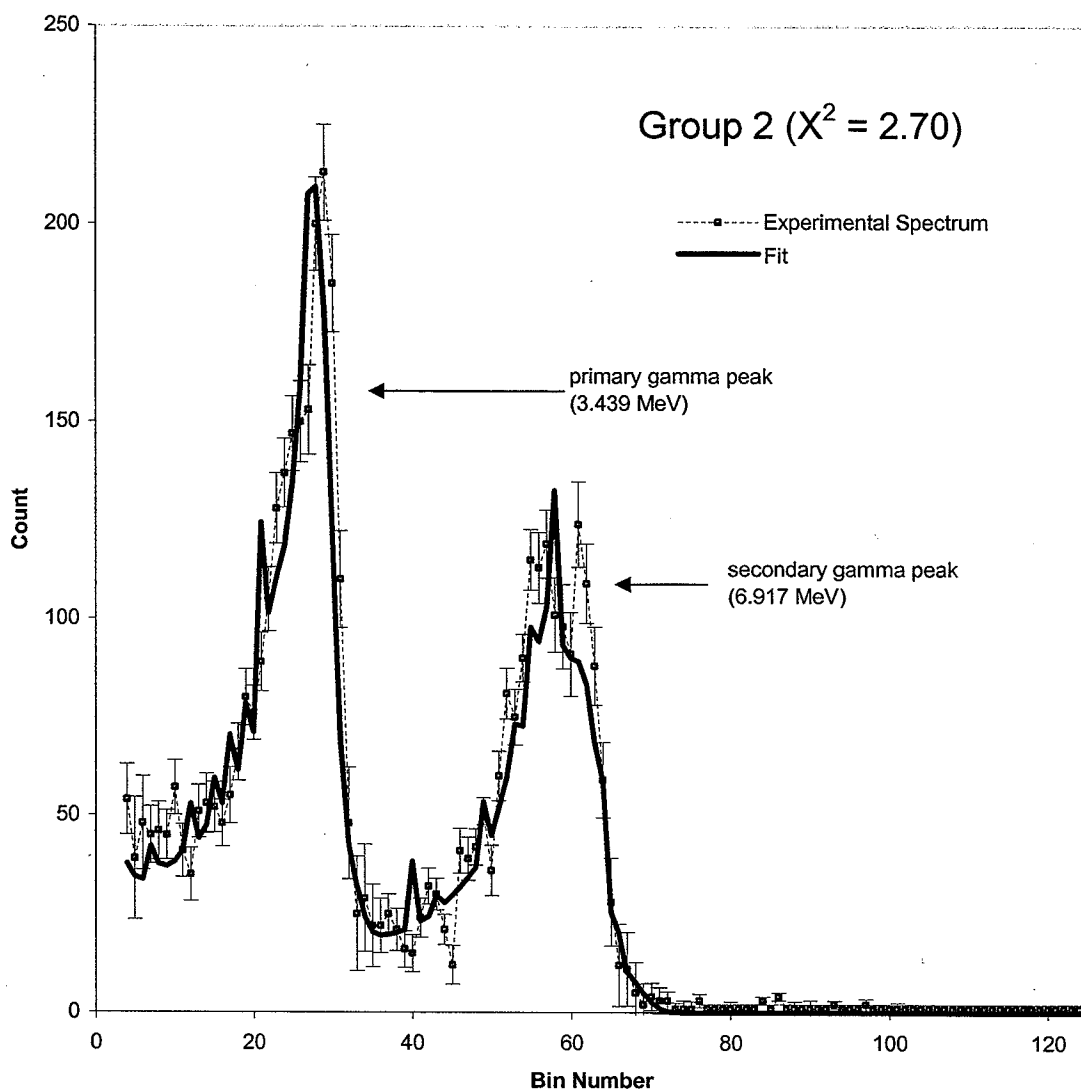


Figure 16b: Group 2 experimental spectrum and Minuit fit performed using maximum gains within allowed errors. Group 2 consists of detectors 13, 14, 15, 16, 17, and 18.

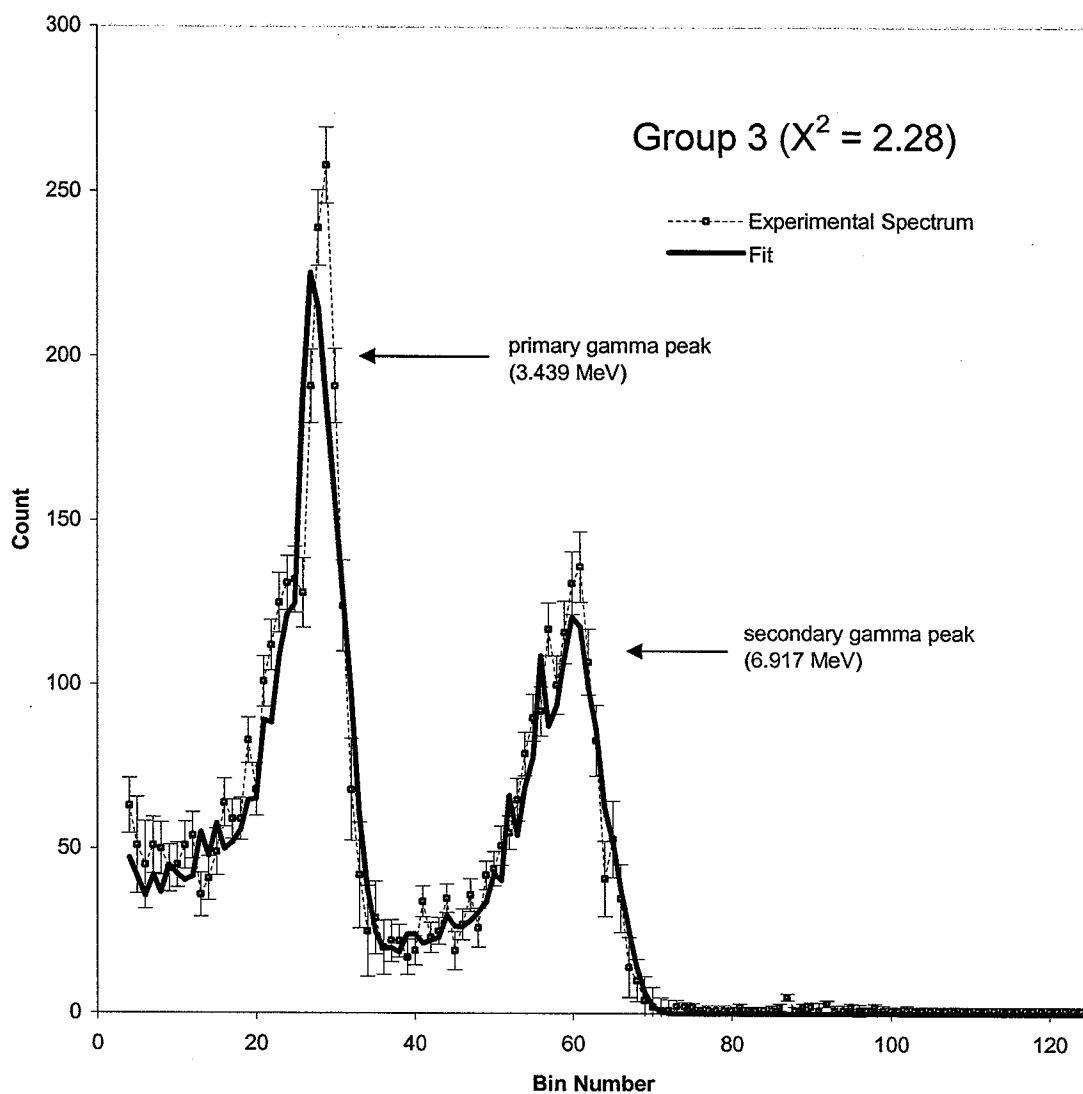


Figure 16c: Group 3 experimental spectrum and Minuit fit performed using maximum gains allowed within errors. Group 3 consists of detectors 5, 6, 19, 20, 21, and 22.

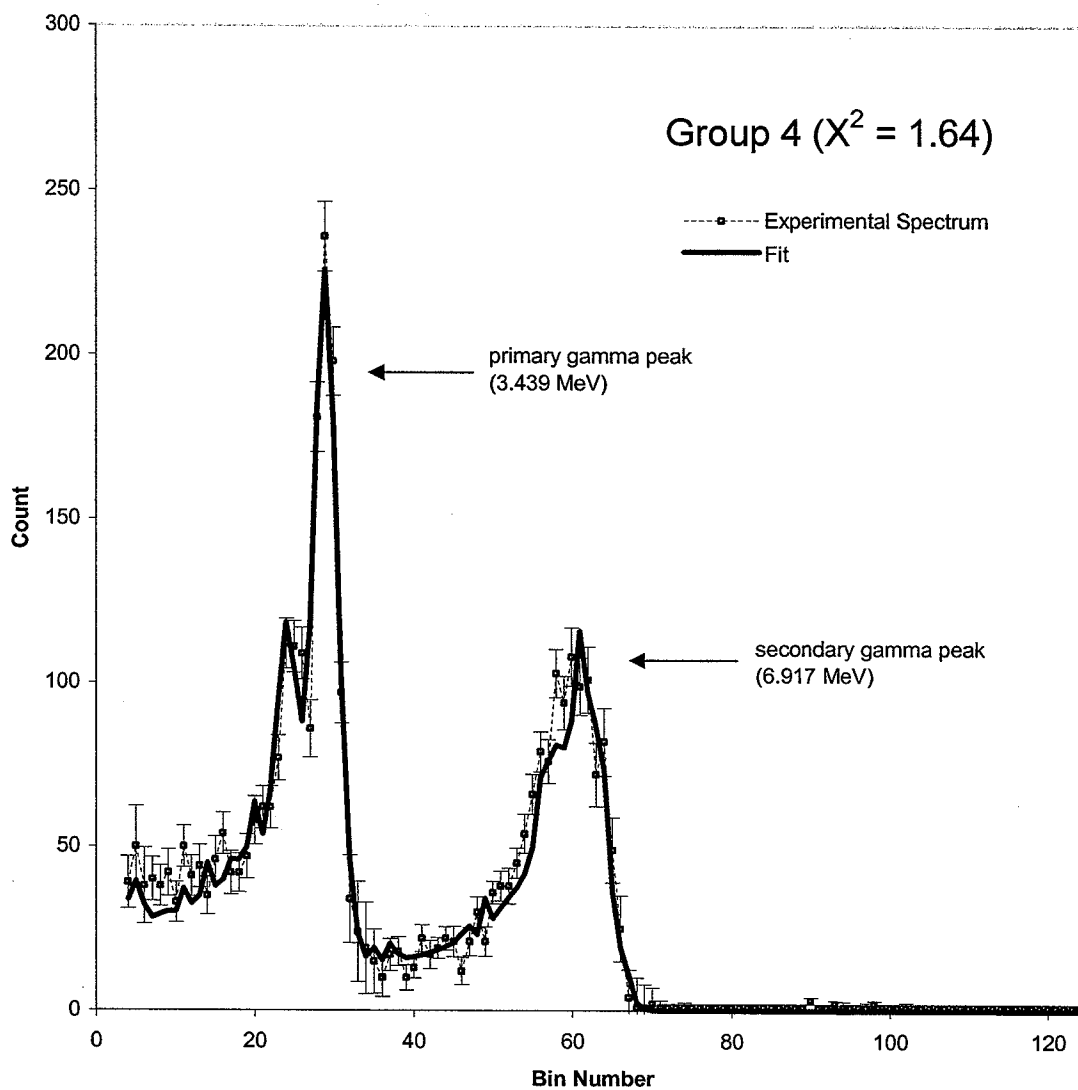


Figure 16d: Group 4 experimental spectrum and Minuit fit performed using maximum gains allowed within errors. Group 4 consists of detectors 23, 24, 25, 26, 27, and 28.

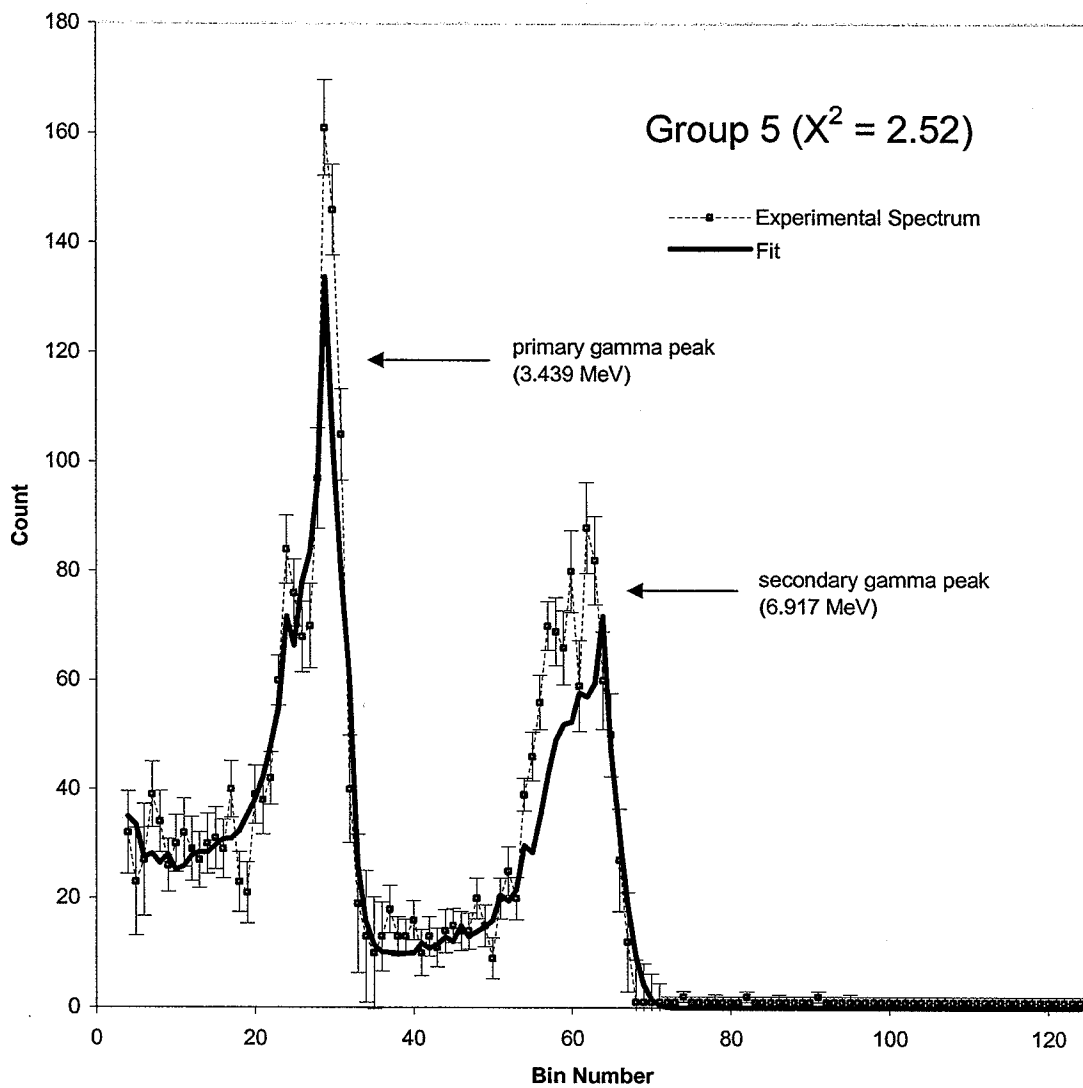


Figure 16e: Group 5 experimental spectrum and Minuit fit performed using maximum gains allowed within errors. Group 5 consists of detectors 7, 8, 9, 10, 29, and 30.

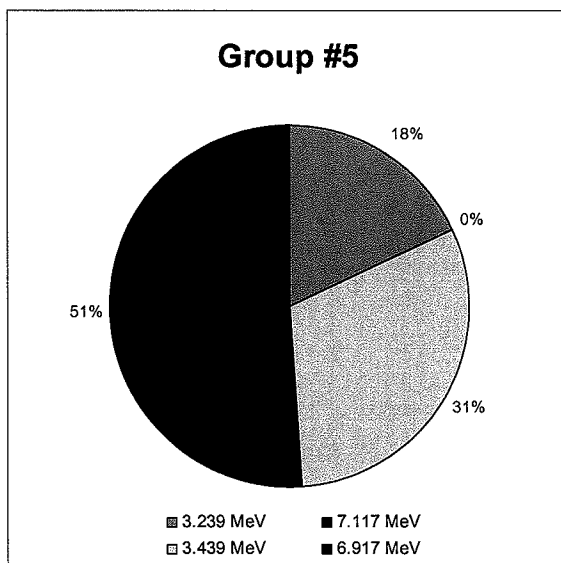
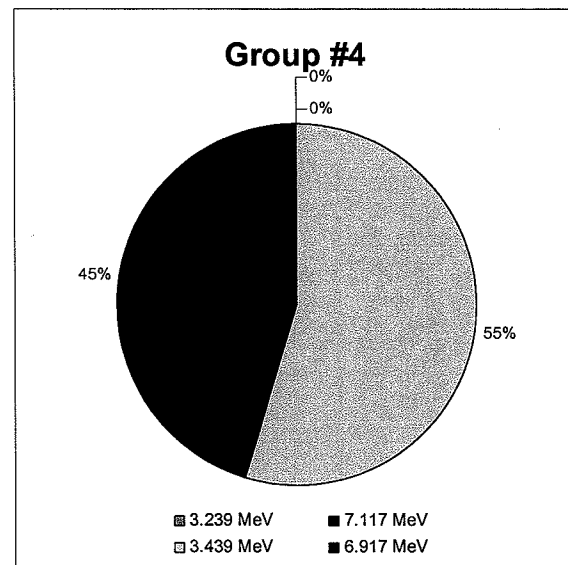
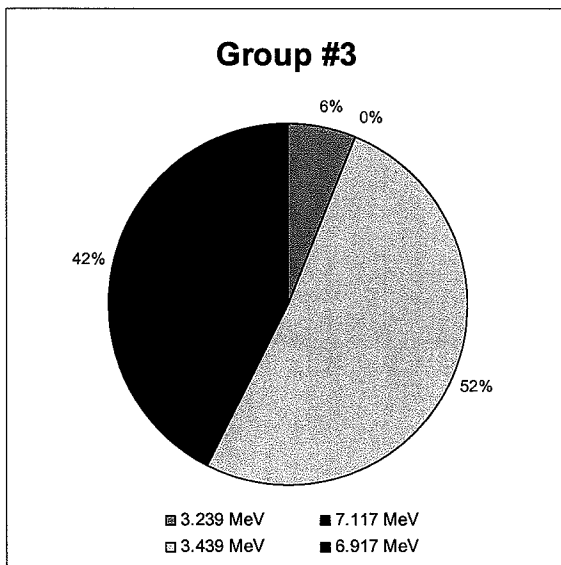
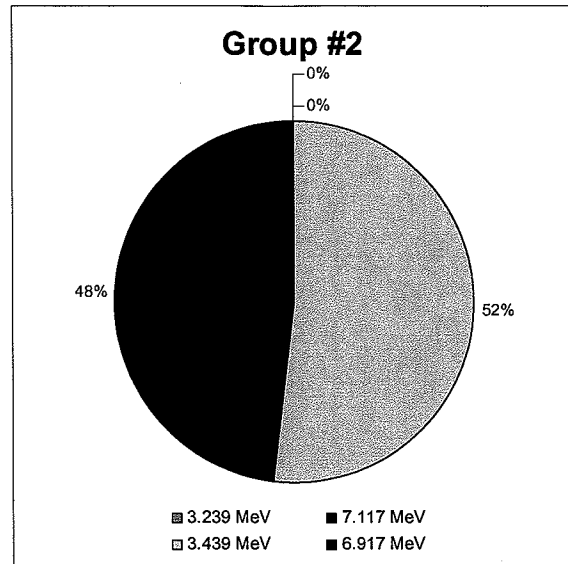
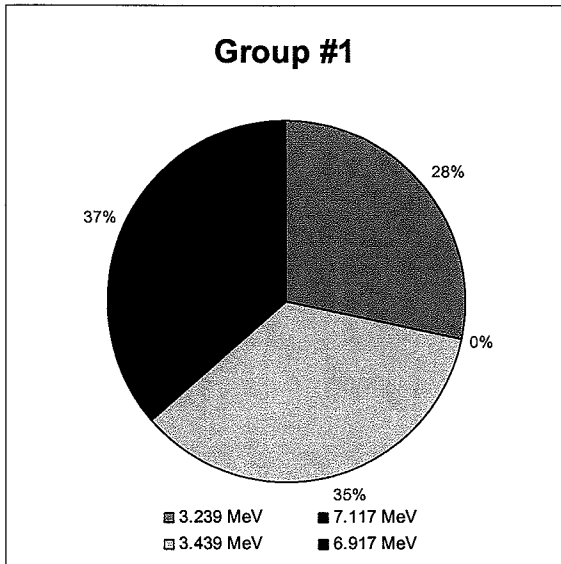


Figure 17: Pie charts showing percentage of each of the four gamma energies present in the fits to the five groups. These were performed using the maximum detector gains allowed within errors. At the 10.356 MeV resonance, ^{16}O decay is known to proceed solely through the 6.917 MeV state; thus only 3.439 MeV (light blue) and 6.917 MeV (dark blue) gammas should appear.

The conclusion is that the method is very sensitive to detector gain and, lacking a better means of finding these gains, gammas produced in decays through the 6.917 and 7.117 MeV states cannot be separated.

If the method cannot separate these states, it cannot be expected to separate the even more closely spaced 6.130 MeV and 6.049 MeV states. If the gains obtained from the 10.356 MeV resonance data, which contains two fairly clear peaks of known energy, are not accurate enough to allow the separation of these states, hopes are slim for data obtained between the resonances, where counts are low and no clear peaks appear.

Why is information about detector gain so elusive? Before data is collected in DRAGON, a gamma source of known energy is placed within the BGO array. The resulting gamma spectrum is observed, and the detector voltages are adjusted such that all detector peaks appear in the same channel. The final voltages are recorded in a file, and data collection proceeds.

However, this calibration is known to be temperature sensitive, and the detector gains are not necessarily maintained over the course of data collection.

This temperature effect is not well understood. Perhaps a solution is to leave the gamma source in the BGO array during data collection. This would create a permanent reference, and changes in detector gain during the course of a run may be noted. Or, perhaps detector calibration should be done both before and after data collection, to get a feeling for how detector gain might have changed during the run.

In any case, the next step in this project must be an effort to better determine detector gains.

4. Conclusions

A method was devised to identify and quantify the discrete components of gamma radiation produced in the $^{12}\text{C}(\alpha,\gamma)^{16}\text{O}$ reaction. The method involves identifying potential ^{16}O decay paths and the gamma energies associated with these paths, generating response functions for these energies, and fitting a linear combination of these response functions to the experimental gamma spectra. Preliminary response functions were generated with GEANT, and to these the effects of detector gain and resolution were added. The fit

coefficients represent the relative strengths of the contributions of each discrete component.

The method was tested on data taken at the 10.356 MeV resonance, at which ^{16}O is known to decay solely through the 6.917 MeV state. Knowing this, two potential decay paths were assumed, these being cascade decay through the 6.917 MeV and 7.117 MeV states. The goal was to test the method at correctly identify gammas produced in decays through closely spaced states.

The test was not successful, with very different results obtained within the error range on the detector gain parameters. The conclusion is that the method is very sensitive to detector gain and, lacking more accurate information about these gains, the devised method cannot accurately identify gammas produced in decays through the 6.917 and 7.117 MeV states. The next step in this project must be an effort to better determine detector gains.

5. References

- [1] D.R. Tilley, H.R. Weller and C.M. Cheves, Nucl. Phys. A, **564** 1 (1993).
- [2] D.G. Gigliotti, Masters Theses, University of Northern British Columbia (to be published).
- [3] D.A. Hutcheon et al., Nucl. Instr. And Meth. A, **192** (2003)

Appendix 1

Energy loss in helium target and the 10.356 MeV resonance

- 1.1 Calculations and discussion
- 1.2 SRIM table

1.1 Calculations and discussion

12C beam energy:	1067	keV/u
	12804	keV
Helium pressure:	8	Torr
	1067	Pa
Helium density:	0.001730548	kg/m ³
	1.73055E-06	kg/cm ³
Geometrical length of target:	11	cm
Energy loss (electrical):	0.001395	MeV/mm
	13.95	keV/cm
	1.1625	keV/u
		cm
Energy loss (nuclear):	9.36E-07	MeV/mm
	9.36E-03	keV/cm
	7.80E-04	keV/u
		cm
Estate:	10356±3	keV
Width:	26±3	keV
Ebeam resonance:	1065±10	keV/u
Formula for beam energy loss within target*:	$E = -1.1625x + 1061$	
Location of resonance:	-3.4±8.6	cm

* distance x is measured from the center of the target

SRIM tables were used to find the electrical and nuclear energy losses, and these are attached. Two facts are omitted in these calculations:

- 1) It is impossible to maintain a perfect vacuum at the entrance and exit apertures of the helium chamber. Thus the effective length of the helium target is somewhat greater than the 11cm geometrical length.
- 2) Gas pressure is not uniform over the length of the target.

The result, that the resonance occurs over a significant portion of the target (-3.4±8.6 cm measured from the center of the target, or from -12.0 cm to 5.2 cm), was used as a rough guideline for the location of the gamma source in the GEANT simulation. This was chosen as a line extending the geometrical length of the target.

1.2 SRIM table

```
=====
Calculation using SRIM-2003
SRIM version ---> SRIM-2003.17
Calc. date ---> August 27, 2003
=====
```

Disk File Name = SRIM Outputs\Carbon in Helium (gas)

Ion = Carbon [6] , Mass = 12 amu

Target Density = 1.7300E-06 g/cm3 = 2.6026E+17 atoms/cm3

Target is a GAS

===== Target Composition =====

Atom Name	Atom Numb	Atomic Percent	Mass Percent
He	2	100.00	100.00

=====

Bragg Correction = 0.00%

Stopping Units = MeV / mm

See bottom of Table for other Stopping units

Ion Energy	dE/dx Elec.	dE/dx Nuclear	Projected Range	Longitudinal Straggling	Lateral Straggling
12.80 MeV	1.395E-03	9.359E-07	9.32 m	269.19 mm	137.26 mm

Multiply Stopping by for Stopping Units

1.0000E-01	eV / Angstrom
1.0000E+00	keV / micron
1.0000E+00	MeV / mm
5.7805E+03	keV / (ug/cm2)
5.7805E+03	MeV / (mg/cm2)
5.7805E+06	keV / (mg/cm2)
3.8424E+04	eV / (1E15 atoms/cm2)
1.1158E+03	L.S.S. reduced units

=====

(C) 1984,1989,1992,1998,2003 by J.P. Biersack and J.F. Ziegler

Appendix 2

Mathematica code

Enter the potential cascade state energies and the 16 O energy (in MeV) :

```
states = {7.117, 6.917};  
E16O = 10.356;  
gammas = {E16O - states[[1]], states[[1]], E16O - states[[2]], states[[2]]}  
  
{3.239, 7.117, 3.439, 6.917}
```

**Import the data files containing the
GEANT results for each gamma energy of interest :**

```
data = Table[Table[0, {i, 1, 30 * 125}], {i, 1, Length[gammas]}}];  
  
data[[1]] = Import["e1067/3239.dat", "TABLE"];  
data[[2]] = Import["standards/7117.dat", "TABLE"];  
data[[3]] = Import["e1067/3439.dat", "TABLE"];  
data[[4]] = Import["standards/6917.dat", "TABLE"];
```

Import the detector gain data :

```
temp = Flatten[Import["e1067/gains.txt", "TABLE"]];  
g = Table[temp[[i]], {i, 1, 30}];  
n = Table[temp[[i]], {i, 31, 60}];
```

Format the GEANT results as required. Note that the matrices d, con, and r are referenced [[gamma #, detector #, bin #]].

```
d = Table[Table[Table[0, {i, 1, 125}], {i, 1, 30}], {i, 1, Length[gamma]}];
con = Table[Table[Table[0, {i, 1, 125}], {i, 1, 30}], {i, 1, Length[gamma]}];
r = Table[Table[Table[0, {i, 1, 125}], {i, 1, 30}], {i, 1, Length[gamma]}];
```

```
For[i = 1, i < Length[gamma],
  For[j = 1, j < 30,
    For[k = 1, k < 125, d[[i, j, k]] = data[[i, j + 30 * (k - 1)]]; k++];
  j++];
  i++];
```

Null⁴

Here are some constants :

```
DeltaE = 12.5 / 125;
halfDeltaE = 12.5 / 250;
energies = Table[halfDeltaE + j * (12.5 / 125), {j, 0, 124}];
photon = 0.511;
factor = Sqrt[8.0 * Log[2]];
```

```
(*kk is the detector resolution parameter*)
kk = 0.1733;
```

Within the following FOR - loop, the response function for each detector, for each gamma energy, is defined.

```

For[y = 1, y ≤ Length[gamma],
  For[z = 1, z ≤ 30,
    detectorNumber = z;
    dofInterest = Flatten[Table[d[[y, detectorNumber, j]], {j, 1, 125}]];
    totalCounts = Sum[dofInterest[[i]], {i, 1, 125}];

    (*perform the convolution*)
    convolution = Table[0, {i, 1, 125}];

    For[i = 1, i ≤ 125,
      sigma = kk * Sqrt[energies[[i]]] / factor;
      gauss = Table[(DeltaE / (sigma * Sqrt[2 π])) * Exp[-(energies[[j]] + halfDeltaE)^2 / (2 * sigma^2)], {j, 1, 124}];
      gaussian = Flatten[Append[Reverse[gauss], (DeltaE / (sigma * Sqrt[2 π]))], gauss]];
      beginIndex = 126;
      gaussianSelection = Table[gaussian[[j]], {j, beginIndex - i, beginIndex + 124 - i}];
      convolution[[i]] = Sum[gaussianSelection[[j]] * dofInterest[[j]], {j, 1, 125}];
      i++;
    ];
    con[[y, detectorNumber]] = convolution;

    (*perform the gain shift*)
    bins = Round[g[[z]] * energies + n[[z]]];
    tot = Table[0, {i, 1, 125}];
    For[i = 1, i ≤ 125,
      If[bins[[i]] > 0, tot[[bins[[i]]]] = tot[[bins[[i]]]] + convolution[[i]]; i++;
    ];
    r[[y, detectorNumber]] = tot;
    z++;
  ];
];

```

Now do the groupings :

```

numGroups = 5;
groupOne = {1, 2, 3, 4, 11, 12};
groupTwo = {13, 14, 15, 16, 17, 18};
groupThree = {5, 6, 19, 20, 21, 22};
groupFour = {23, 24, 25, 26, 27, 28};
groupFive = {7, 8, 29, 30, 9, 10};

rr = Table[Table[Table[0, {i, 1, 125}], {i, 1, numGroups}], {i, 1, Length[gamma]}];

For[i = 1, i < Length[gamma],
  rr[[i, 1]] = Sum[r[[i, groupOne[[j]]], {j, 1, Length[groupOne]}];
  rr[[i, 2]] = Sum[r[[i, groupTwo[[j]]], {j, 1, Length[groupTwo]}];
  rr[[i, 3]] = Sum[r[[i, groupThree[[j]]], {j, 1, Length[groupThree]}];
  rr[[i, 4]] = Sum[r[[i, groupFour[[j]]], {j, 1, Length[groupFour]}];
  rr[[i, 5]] = Sum[r[[i, groupFive[[j]]], {j, 1, Length[groupFive]}];
  i++];

(*Normalize*)
For[i = 1, i < Length[gamma],
  For[j = 1, j < numGroups,
    rr[[i, j]] = rr[[i, j]] / 100000;
    (*100000 is the number of events of each gamma energy generated*)
    j++;
  i++];

dat = Import["e1067/8217.dat", "TABLE"];

```

Summary : the output is the matrix rr, which is referenced rr[[gamma #, group #, bin #]].

Import and format the data for the run of interest :

```

d = Table[Table[0, {i, 1, 125}], {i, 1, 30}];
For[j = 1, j ≤ 125, d[[30, j]] = dat[[j]]; j++];
For[i = 1, i ≤ 29, For[j = 1, j ≤ 125, d[[i, j]] = dat[[125 * i + j]]; j++];
i++];

```

(*In the table 'input' the raw data is grouped into the five groups defined previously.*)

```

input = Table[Table[0, {i, 1, 125}], {i, 1, numGroups}];

input[[1]] = Flatten[Sum[d[[groupOne[[i]]]], {i, 1, Length[groupOne]}]];
input[[2]] = Flatten[Sum[d[[groupTwo[[i]]]], {i, 1, Length[groupTwo]}]];
input[[3]] = Flatten[Sum[d[[groupThree[[i]]]], {i, 1, Length[groupThree]}]];
input[[4]] = Flatten[Sum[d[[groupFour[[i]]]], {i, 1, Length[groupFour]}]];
input[[5]] = Flatten[Sum[d[[groupFive[[i]]]], {i, 1, Length[groupFive]}]];

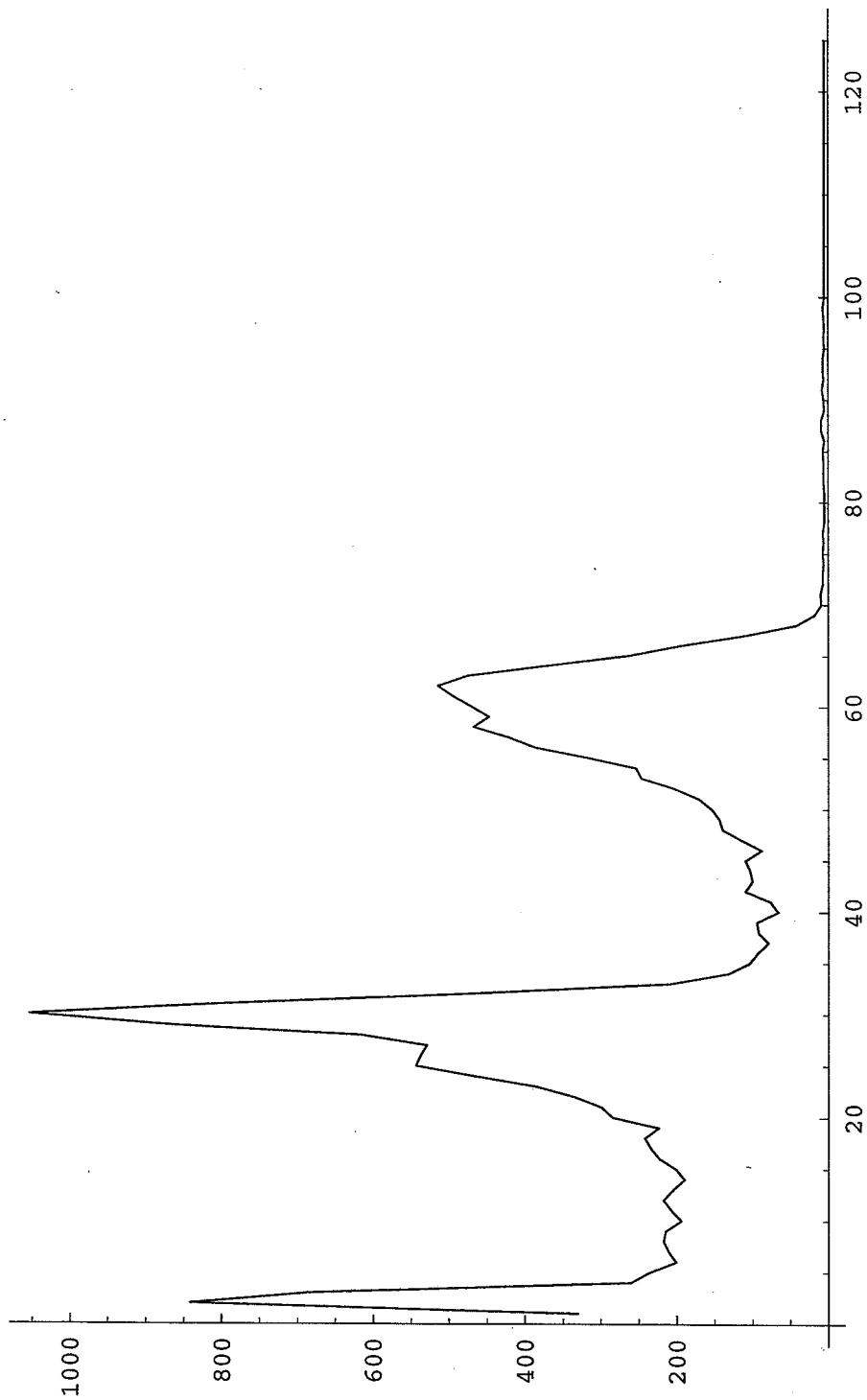
For[i = 1, i ≤ numGroups,
  For[j = 1, j ≤ 125,
    If[input[[i, j]] = 0, input[[i, j]] = 1];
    j++;
  i++];

```

Now have a look at the data :


```
<< Graphics`MultipleListPlot`
```

```
t = input[[1]] + input[[2]] + input[[3]] + input[[4]] + input[[5]];
ListPlot[t, PlotJoined -> True, PlotRange -> All]
```



- Graphics -

- Graphics -

Define the desired bin range for fitting. 'Low' is the lowest bin of interest, while 'high' is the highest. The data in this range is stored in the table 'inputRev.'

```
low = 5;  
high = 125;  
inputRev = Table[Table[0, {i, 1, (high - low + 1)}], {i, 1, numGroups}];  
  
For[i = 1, i ≤ numGroups,  
  inputRev[[i]] = Table[input[[i, j]], {j, low, high}]; i++]
```

Null⁴

Now prepare the output files ...

numPoints = high - low + 1

121

```

output1 = Table[0, {i, 1, numPoints*5}];
For[i = 1, i ≤ numPoints, output1[[i]] = inputRev[[1, i]]; i++];
For[i = numPoints + 1, i ≤ 2 * numPoints, output1[[i]] = rr[[1, 1, i - numPoints + low - 1]]; i++];
For[i = 2 * numPoints + 1, i ≤ 3 * numPoints, output1[[i]] = rr[[2, 1, i - 2 * numPoints + low - 1]]; i++];
For[i = 3 * numPoints + 1, i ≤ 4 * numPoints, output1[[i]] = rr[[3, 1, i - 3 * numPoints + low - 1]]; i++];
For[i = 4 * numPoints + 1, i ≤ 5 * numPoints, output1[[i]] = rr[[4, 1, i - 4 * numPoints + low - 1]]; i++];

output2 = Table[0, {i, 1, numPoints*10}];
For[i = 1, i ≤ numPoints, output2[[i]] = inputRev[[2, i]]; i++];
For[i = numPoints + 1, i ≤ 2 * numPoints, output2[[i]] = rr[[1, 2, i - numPoints + low - 1]]; i++];
For[i = 2 * numPoints + 1, i ≤ 3 * numPoints, output2[[i]] = rr[[2, 2, i - 2 * numPoints + low - 1]]; i++];
For[i = 3 * numPoints + 1, i ≤ 4 * numPoints, output2[[i]] = rr[[3, 2, i - 3 * numPoints + low - 1]]; i++];
For[i = 4 * numPoints + 1, i ≤ 5 * numPoints, output2[[i]] = rr[[4, 2, i - 4 * numPoints + low - 1]]; i++];

output3 = Table[0, {i, 1, numPoints*10}];
For[i = 1, i ≤ numPoints, output3[[i]] = inputRev[[3, i]]; i++];
For[i = numPoints + 1, i ≤ 2 * numPoints, output3[[i]] = rr[[1, 3, i - numPoints + low - 1]]; i++];
For[i = 2 * numPoints + 1, i ≤ 3 * numPoints, output3[[i]] = rr[[2, 3, i - 2 * numPoints + low - 1]]; i++];
For[i = 3 * numPoints + 1, i ≤ 4 * numPoints, output3[[i]] = rr[[3, 3, i - 3 * numPoints + low - 1]]; i++];
For[i = 4 * numPoints + 1, i ≤ 5 * numPoints, output3[[i]] = rr[[4, 3, i - 4 * numPoints + low - 1]]; i++];

output4 = Table[0, {i, 1, numPoints*10}];
For[i = 1, i ≤ numPoints, output4[[i]] = inputRev[[4, i]]; i++];
For[i = numPoints + 1, i ≤ 2 * numPoints, output4[[i]] = rr[[1, 4, i - numPoints + low - 1]]; i++];
For[i = 2 * numPoints + 1, i ≤ 3 * numPoints, output4[[i]] = rr[[2, 4, i - 2 * numPoints + low - 1]]; i++];
For[i = 3 * numPoints + 1, i ≤ 4 * numPoints, output4[[i]] = rr[[3, 4, i - 3 * numPoints + low - 1]]; i++];
For[i = 4 * numPoints + 1, i ≤ 5 * numPoints, output4[[i]] = rr[[4, 4, i - 4 * numPoints + low - 1]]; i++];

output5 = Table[0, {i, 1, numPoints*10}];
For[i = 1, i ≤ numPoints, output5[[i]] = inputRev[[5, i]]; i++];
For[i = numPoints + 1, i ≤ 2 * numPoints, output5[[i]] = rr[[1, 5, i - numPoints + low - 1]]; i++];
For[i = 2 * numPoints + 1, i ≤ 3 * numPoints, output5[[i]] = rr[[2, 5, i - 2 * numPoints + low - 1]]; i++];
For[i = 3 * numPoints + 1, i ≤ 4 * numPoints, output5[[i]] = rr[[3, 5, i - 3 * numPoints + low - 1]]; i++];
For[i = 4 * numPoints + 1, i ≤ 5 * numPoints, output5[[i]] = rr[[4, 5, i - 4 * numPoints + low - 1]]; i++];

Export["minuit/gfstunres/g1.dat", output1, "LIST"];
Export["minuit/gfstunres/g2.dat", output2, "LIST"];
Export["minuit/gfstunres/g3.dat", output3, "LIST"];
Export["minuit/gfstunres/g4.dat", output4, "LIST"];
Export["minuit/gfstunres/g5.dat", output5, "LIST"];

```

Type in the fit coefficients to visualize the fit :

```

gNum = 1;
c = {0, 20283, 14242, 3691.8};
f1 = c[[1]] * rr[[1, gNum]] + c[[2]] * rr[[2, gNum]] + c[[3]] * rr[[3, gNum]] + c[[4]] * rr[[4, gNum]];

gNum = 2;
c = {0, 15179, 13178, 0};
f2 = c[[1]] * rr[[1, gNum]] + c[[2]] * rr[[2, gNum]] + c[[3]] * rr[[3, gNum]] + c[[4]] * rr[[4, gNum]];

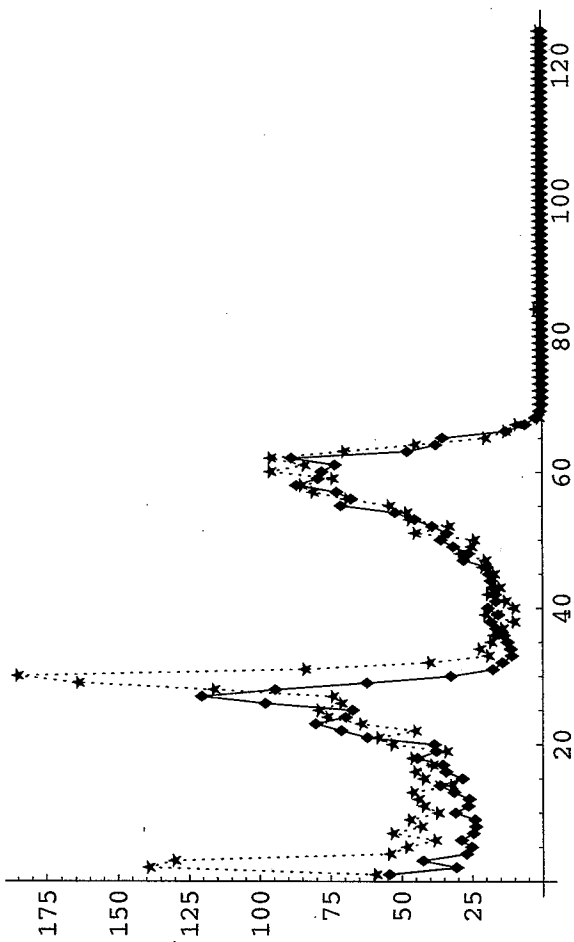
gNum = 3;
c = {0, 10550, 11479, 0};
f3 = c[[1]] * rr[[1, gNum]] + c[[2]] * rr[[2, gNum]] + c[[3]] * rr[[3, gNum]] + c[[4]] * rr[[4, gNum]];

gNum = 4;
c = {0, 3405.2, 12337, 6003.9};
f4 = c[[1]] * rr[[1, gNum]] + c[[2]] * rr[[2, gNum]] + c[[3]] * rr[[3, gNum]] + c[[4]] * rr[[4, gNum]];

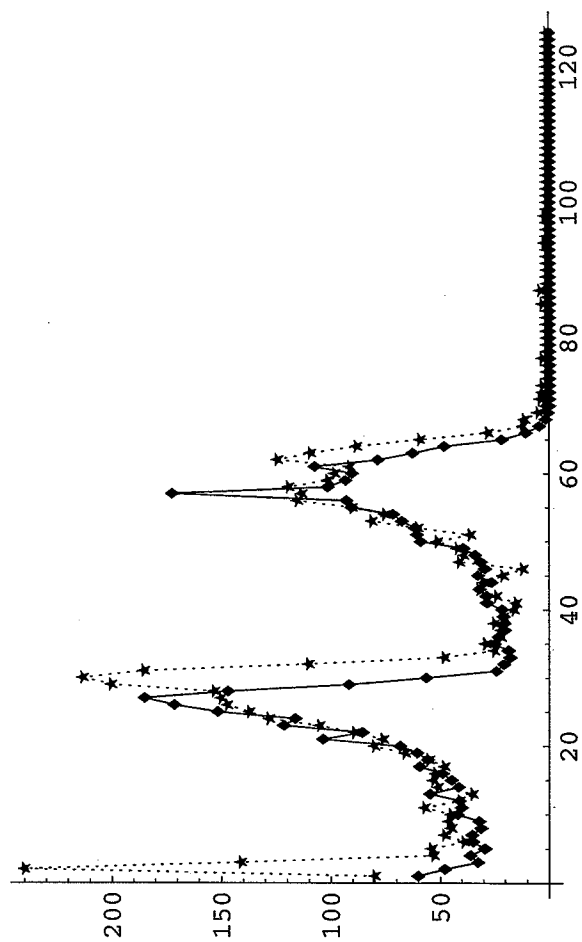
gNum = 5;
c = {36.643, 26143, 15868, 0};
f5 = c[[1]] * rr[[1, gNum]] + c[[2]] * rr[[2, gNum]] + c[[3]] * rr[[3, gNum]] + c[[4]] * rr[[4, gNum]];

MultipleListPlot[f1, input[[1]], PlotRange → All, PlotJoined → True]
MultipleListPlot[f2, input[[2]], PlotRange → All, PlotJoined → True]
MultipleListPlot[f3, input[[3]], PlotRange → All, PlotJoined → True]
MultipleListPlot[f4, input[[4]], PlotRange → All, PlotJoined → True]
MultipleListPlot[f5, input[[5]], PlotRange → All, PlotJoined → True]
MultipleListPlot[f1 + f2 + f3 + f4 + f5,
  input[[1]] + input[[2]] + input[[3]] + input[[4]] + input[[5]], PlotRange → All, PlotJoined → True]

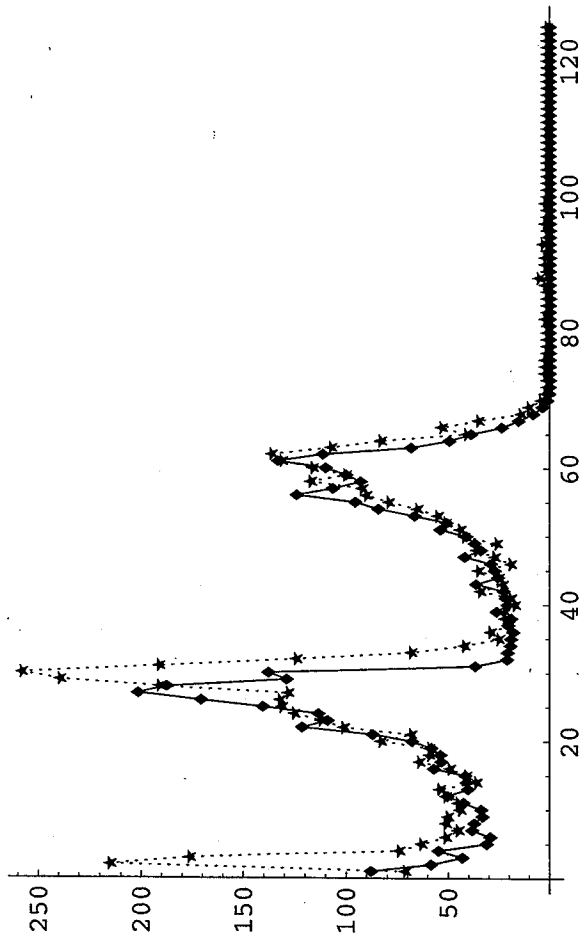
```



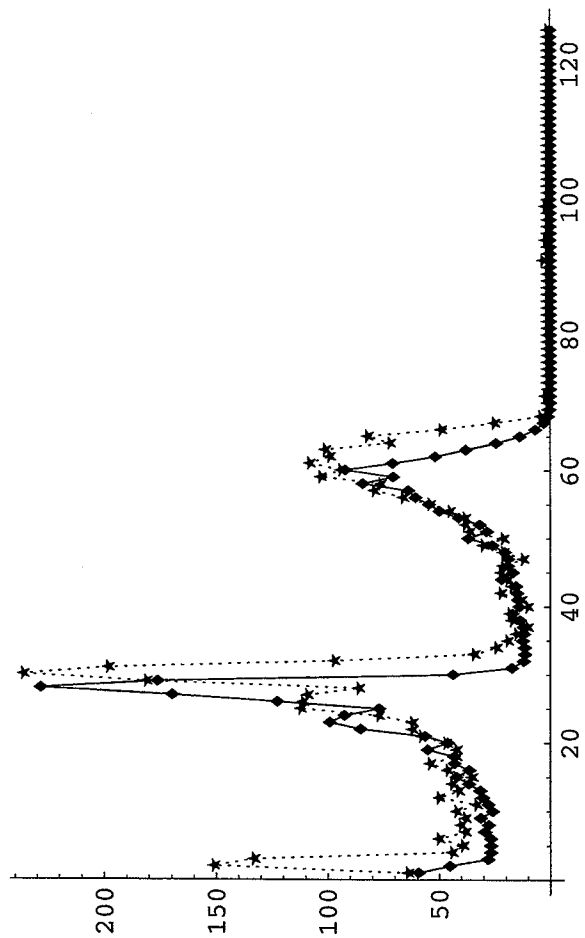
- Graphics -



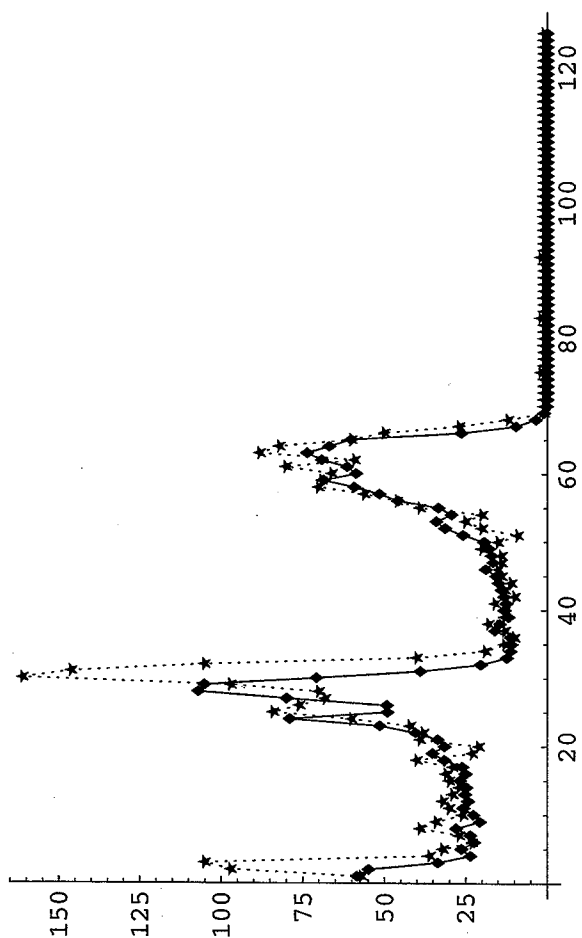
- Graphics -



- Graphics -



- Graphics -



Appendix 3

Detector gain parameters

- 3.1 Bin numbers of 3.439 MeV and 6.917 MeV peaks
- 3.2 Gain parameters g and N
- 3.3 Minuit code for finding gain parameters g and N

3.1 Bin numbers of 3.439 MeV and 6.917 MeV peaks

Detector Number	3.439 MeV peak bin number	+/-	6.917 MeV peak bin number	+/-
1	28.110	0.38107	61.625	0.92935
2	27.260	0.57059	61.282	0.48164
3	27.266	0.47086	59.442	0.51802
4	26.424	0.79143	58.183	0.82929
5	29.424	0.37543	63.146	0.38429
6	27.169	0.32369	58.550	0.32788
7	28.675	0.61189	61.079	0.77597
8	28.128	0.59182	60.570	0.58811
9	28.822	0.34423	61.864	0.36950
10	28.323	0.41517	60.528	0.33561
11	23.133	2.41020	56.963	0.37004
12	27.993	0.38405	58.659	0.36684
13	26.428	0.73600	59.089	0.48263
14	28.482	0.53324	61.566	1.15860
15	26.959	0.38235	58.421	0.29952
16	28.185	0.38373	59.668	0.33054
17	24.817	0.42626	55.440	0.21527
18	27.280	0.28976	59.980	0.31646
19	26.629	0.42841	54.344	2.24410
20	25.947	1.15610	59.090	0.64642
21	27.659	0.30573	58.896	0.36708
22	26.948	0.26623	58.764	0.26104
23	27.570	0.38360	59.245	0.57491
24	27.529	0.43420	60.080	0.30381
25	27.695	0.45382	58.567	0.44513
26	27.249	0.73058	58.525	0.99038
27	27.415	0.30140	60.640	0.49359
28	28.305	0.30938	61.696	0.29651
29	29.005	0.37256	61.454	0.50867
30	27.540	0.28070	60.856	0.35404

3.2 Gain parameters g and N

Detector Number	g	+/-	N	+/-
1	9.6307	0.44735	-5.0198	1.8491
2	9.7764	0.33319	-6.3709	1.9102
3	9.2459	0.31264	-4.5404	1.6561
4	9.1261	0.48783	-4.9699	2.6237
5	9.6902	0.23699	-3.9103	1.3001
6	9.0175	0.24124	-3.8513	1.3071
7	9.3115	0.46385	-3.3566	2.3539
8	9.3224	0.37213	-3.9411	2.0448
9	9.4948	0.15307	-3.8405	0.85437
10	9.2543	0.20614	-3.5115	1.1941
11	9.7218	0.4713	-10.312	3.231
12	8.812	0.23659	-2.3209	1.3128
13	9.3854	0.39713	-5.8578	2.4151
14	9.5069	0.53891	-4.2216	2.3027
15	9.0408	0.18747	-4.1415	1.1034
16	9.0468	0.22568	-2.9365	1.2907
17	8.7999	0.21213	-5.4549	1.3554
18	9.3965	0.18959	-5.0441	1.0056
19	7.9641	1.0203	-0.7675	3.6888
20	9.5239	0.59023	-6.8152	3.7039
21	8.9762	0.23764	-3.2191	1.2269
22	9.1425	0.15028	-4.5024	0.81728
23	9.1021	0.26477	-3.7406	1.3115
24	9.3537	0.23595	-4.6478	1.4198
25	8.8713	0.28334	-2.8222	1.558
26	8.9874	0.57367	-3.6675	2.8437
27	9.5475	0.28334	-5.4283	1.3312
28	9.5951	0.1876	-4.7023	1.043
29	9.3244	0.28121	-3.0712	1.39
30	9.5736	0.25432	-5.3931	1.2831

3.3 Minuit code for finding gain parameters g and N

main.f

```
PROGRAM MAIN
EXTERNAL FCNGAMMA
OPEN (5,FILE='gin.dat',STATUS='OLD')
OPEN (6,FILE='gout.dat',STATUS='OLD')
CALL MINTIO(5,6,7)
CALL MINUIT(FCNGAMMA,0)
STOP
END
```

fcngamma.f

```
SUBROUTINE FCNGAMMA(NPAR,GRAD,FVAL,XVAL,IFLAG,FUTIL)
IMPLICIT DOUBLE PRECISION (A-H,O-Z)
DIMENSION GRAD(*),XVAL(*)
INTEGER i, j
PARAMETER (npoints = 4)
PARAMETER (np = 2)
REAL d(npoints)
REAL p(np)

C
C   open(3,FILE='data.dat',STATUS='OLD')
C
C   do 100 i = 1, npoints
C       read(3,*) d(i)
100 continue
C       close(3)
C
C   FVAL = 0.0
C
C   do 400 i=1, np
C       p(i) = XVAL(i)
400 continue
C
C   FVAL = ((p(1)*3.44+p(2)-d(1))/d(2))**2
C   $ + ((p(1)*6.92 + p(2) - d(3))/d(4))**2
C
C   RETURN
END
```

gin.dat

```
set title
GAMMA FITTER
parameters
1 'slope' 1.0 0.1
2 'intercept' 1.0 0.1
```

```
error def 2.41
migrad
minos
```

data.dat

```
27.540
0.28070
60.856
0.35404
```

Appendix 4

Minuit code for linear fit of response functions to
experimental gamma spectra

Minuit code for linear fit of response functions to experimental gamma spectra

main.f

```
PROGRAM MAIN
EXTERNAL FCNGAMMA
OPEN (5,FILE='gin.dat',STATUS='OLD')
OPEN (6,FILE='gout.dat',STATUS='OLD')
CALL MINTIO(5,6,7)
CALL MINUIT(FCNGAMMA,0)
STOP
END
```

fcngamma.f

```
SUBROUTINE FCNGAMMA(NPAR,GRAD,FVAL,XVAL,IFLAG,FUTIL)
IMPLICIT DOUBLE PRECISION (A-H,O-Z)
DIMENSION GRAD(*),XVAL(*)
INTEGER i, j
PARAMETER (ngammas = 4)
PARAMETER (npoints = 121)
PARAMETER (np = 4)
REAL rr(ngammas,npoints)
REAL d(npoints)
REAL p(np), t

C
open(3,FILE='data.dat',STATUS='OLD')
C
do 100 i = 1, npoints
  read(3,*) d(i)
100 continue
C
C
do 300 j = 1, ngammas
  do 20 i = 1, npoints
    read(3,*) rr(j,i)
  20 continue
300 continue
close(3)
C
FVAL = 0.0
t = 0.0
C
do 400 i=1, np
  p(i) = XVAL(i)
400 continue
C
do 500 i=1, npoints
  t = 0.0
  t = t + p(1)*rr(1,i) + p(2)*rr(2,i) + p(3)*rr(3,i)
  $ + p(4)*rr(4,i)
  FVAL = FVAL+(t-d(i))*(t-d(i))/d(i)
500 continue
C
```

RETURN
END

gin.dat

```
set title
GAMMA FITTER
parameters
1 '3239' 1.0 1.0 0.0 1000000.0
2 '7117' 1.0 1.0 0.0 1000000.0
3 '3439' 1.0 1.0 0.0 1000000.0
4 '6917' 1.0 1.0 0.0 1000000.0
```

```
error def 4.88
migrad
minos
```